Quality-Controlled Upper-Air Sounding Dataset for DYNAMO/CINDY/AMIE: Development and Corrections

PAUL E. CIESIELSKI,* HUNGJUI YU,* RICHARD H. JOHNSON,* KUNIO YONEYAMA,+ MASAKI KATSUMATA,+ CHARLES N. LONG,# JUNHONG WANG,@ SCOT M. LOEHRER,& KATHRYN YOUNG,& STEVEN F. WILLIAMS,& WILLIAM BROWN,& JOHN BRAUN,** AND TERESA VAN HOVE**

* *Department of Atmospheric Science, Colorado State University, Fort Collins, Colorado*
+ *Japanese Agency for Marine-Earth Science and Technology, Yokosuka, Japan*
# *Pacific Northwest National Laboratory, Richland, Washington*
@ *Department of Atmospheric and Environmental Sciences, University at Albany, State University of New York, Albany, New York, and National Center for Atmospheric Research, Boulder, Colorado*
& *National Center for Atmospheric Research, Boulder, Colorado*
** *University Corporation for Atmospheric Research, Boulder, Colorado*

(Manuscript received 5 August 2013, in final form 8 January 2014)

ABSTRACT

The upper-air sounding network for Dynamics of the Madden–Julian Oscillation (DYNAMO) has provided an unprecedented set of observations for studying the MJO over the Indian Ocean, where coupling of this oscillation with deep convection first occurs. With 72 rawinsonde sites and dropsonde data from 13 aircraft missions, the sounding network covers the tropics from eastern Africa to the western Pacific. In total nearly 26 000 soundings were collected from this network during the experiment's 6-month extended observing period (from October 2011 to March 2012). Slightly more than half of the soundings, collected from 33 sites, are at high vertical resolution. Rigorous post–field phase processing of the sonde data included several levels of quality checks and a variety of corrections that address a number of issues (e.g., daytime dry bias, baseline surface data errors, ship deck heating effects, and artificial dry spikes in slow-ascent soundings).

Because of the importance of an accurate description of the moisture field in meeting the scientific goals of the experiment, particular attention is given to humidity correction and its validation. The humidity corrections, though small relative to some previous field campaigns, produced high-fidelity moisture analyses in which sonde precipitable water compared well with independent estimates. An assessment of operational model moisture analyses using corrected sonde data shows an overall good agreement with the exception at upper levels, where model moisture and clouds are more abundant than the sonde data would indicate.

1. Introduction

As a result of limitations in our basic understanding of and ability to predict the MJO, particularly its initiation, a field campaign was recently conducted in the Indian Ocean (IO) region during the period October 2011–March 2012 (Yoneyama et al. 2013). The experiment was composed of three principal components: Dynamics of the Madden–Julian Oscillation (DYNAMO), Cooperative Indian Ocean Experiment on Intraseasonal Variability in the Year 2011 (CINDY2011), and Atmospheric Radiation Measurement (ARM) MJO Investigation Experiment (AMIE). Hereafter, the collective field campaign effort will be referred to as DYNAMO.

Because of the large-scale nature of the MJO, an enhanced upper-air sounding network was established over the IO region (Fig. 1) that extended zonally from eastern Africa to the western Pacific. Observations from this network will allow the study of MJO initiation over the IO, where its deep convection signal is first observed, and its subsequent evolution over the Maritime Continent and western Pacific warm pool region. A primary component of this enhanced network were six core sounding sites in central IO that formed two quadrilateral sounding arrays, one north and one south of the equator. These two arrays

Corresponding author address: Paul E. Ciesielski, Department of Atmospheric Science, Colorado State University, 1371 Campus Delivery, Fort Collins, CO 80523.
E-mail: paulc@atmos.colostate.edu

DOI: 10.1175/JTECH-D-13-00165.1

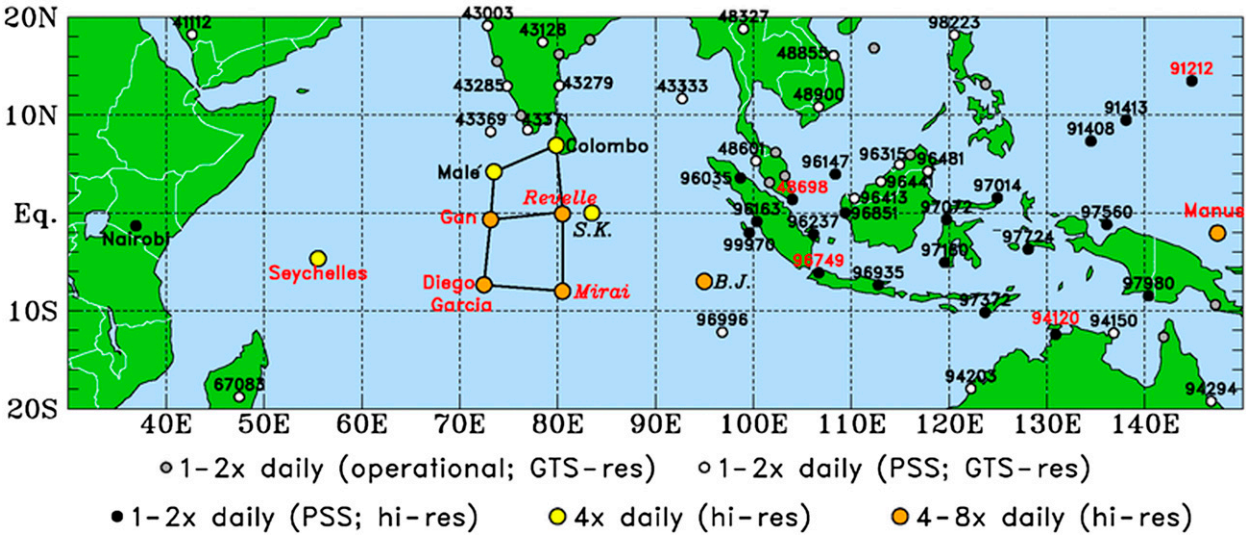

FIG. 1. Upper-air sounding network for DYNAMO where color coding of dots indicates the type of site, including typical launch frequency. Enhanced sounding sites are labeled with station name, while PSS are labeled with WMO number. Red labels indicate sites with collocated GPS and/or MWR PW data. High-resolution sonde data were collected at 11 enhanced sites and 21 PSS (black dots).

will provide the observations necessary for diagnostic studies of heat and moisture budgets from which the properties of convection can be inferred (Yanai et al. 1973). In addition, the data allow for the computation of advective properties of heat and moisture to force cloud-resolving models and single-column models, which aids in the improvement of parameterization schemes (Wu et al. 2000).

Building on the success of past tropical field campaigns, most notably the Global Atmospheric Research Program Atlantic Tropical Experiment (GATE) in 1973 (International and Scientific Management Group of GATE 1974) and the Tropical Ocean and Global Atmosphere Coupled Ocean–Atmosphere Response Experiment (TOGA COARE) in 1992–93 (Webster and Lukas 1992), DYNAMO provides scientifically important observations over data-sparse regions of our planet. In addition to the important budget applications cited above, these sounding networks provide the observations needed to describe environmental conditions that provide a context for validating and understanding other observations (radar, satellite, etc.), to initialize models for reanalyses and case studies, and to validate models. In particular, high-vertical-resolution (hi-res) DYNAMO sounding observations will be instrumental in achieving the stated goal of determining the mechanisms by which the troposphere is moistened in the initiation stage of the MJO.

Considering the wide use of the sounding dataset and the requirement for high-quality observations to meet the experimental goals, a special effort was undertaken to create the "best possible" set of sounding observations. The purpose of this paper is to document the performance and characteristics of the DYNAMO upper-air sounding network (section 2), and to describe the quality-control (QC) procedures (section 3) and corrections to the sonde data (section 4). Our confidence in the accuracy of the sonde humidity observations shown in sections 4 and 5 allows us to use them as a tool to evaluate the reliability of some satellite- and model-based moisture products (section 5). Summary comments are provided in section 6.

2. Upper-air network overview and other data sources

a. *Sounding inventory*

While data collection for a few DYNAMO sites began as early as September 2011, most sites began observations around 1 October 2011. This date marked the formal beginning of three noteworthy observing periods for the experiment, which are summarized in Table 1. In general, the best data coverage for both arrays occurred during the special observing period (SOP) from early October through the end of November, during which time two robust MJOs passed over the network (Johnson and Ciesielski 2013). A visual inventory of the six core sites is shown in Fig. 2. From this plot we note that the southern sounding array (SSA; bottom four panels) was configured to achieve eight soundings per day in a quadrilateral network through the end of the SOP, after which it was triangular shaped with four soundings per day when the Research Vessel (R/V) *Mirai* departed and the R/V *Revelle* was on site. On the other hand, the northern sounding array (NSA; top four panels) was configured as a quadrilateral through 15 December when the *Revelle* was on site and triangular when not. The typical launch

TABLE 1. Dates for various observing periods in DYNAMO. IOP is the intensive observing period.

Name	Dates	Comments
SOP	1 Oct 11–30 Nov 2011	SSA launched at 3-h frequency
IOP	1 Oct 11–15 Jan 2012	After SOP, *Mirai* off-site, *Revelle* and Diego at 6-h frequency
EOP	1 Oct 11–31 Mar 2012	Gan to 1–2 soundings per day after 9 Feb

frequency at Malé, Republic of Maldives, and Colombo, Sri Lanka, was four soundings per day during the SOP; however, after 5 December the frequency at Colombo was reduced to one sounding per day.

Sounding operations at 11 sites in the DYNAMO domain (including the six core sites) were enhanced either by increasing the sounding frequency above normal operational frequency or establishing operations where none previously existed. Hi-res data were collected for these 11 sites, which are labeled with their station names in Fig. 1 and highlighted in boldface in Table 2. Two of the enhanced sites at Diego Garcia and R/V *Revelle* deployed a National Center for Atmospheric Research (NCAR) Integrated Sounding System (ISS) that included a surface meteorological (SMET) station, a 915-MHz wind profiler, a GPS Advanced Upper-Air Sounding System (GAUS), and a ground-based GPS receiver for computation of total-column precipitable water (PW). As part of the ISS at Diego Garcia, a radio acoustic sounding system (RASS) was also deployed to retrieve virtual temperature profiles up to about 1 km.

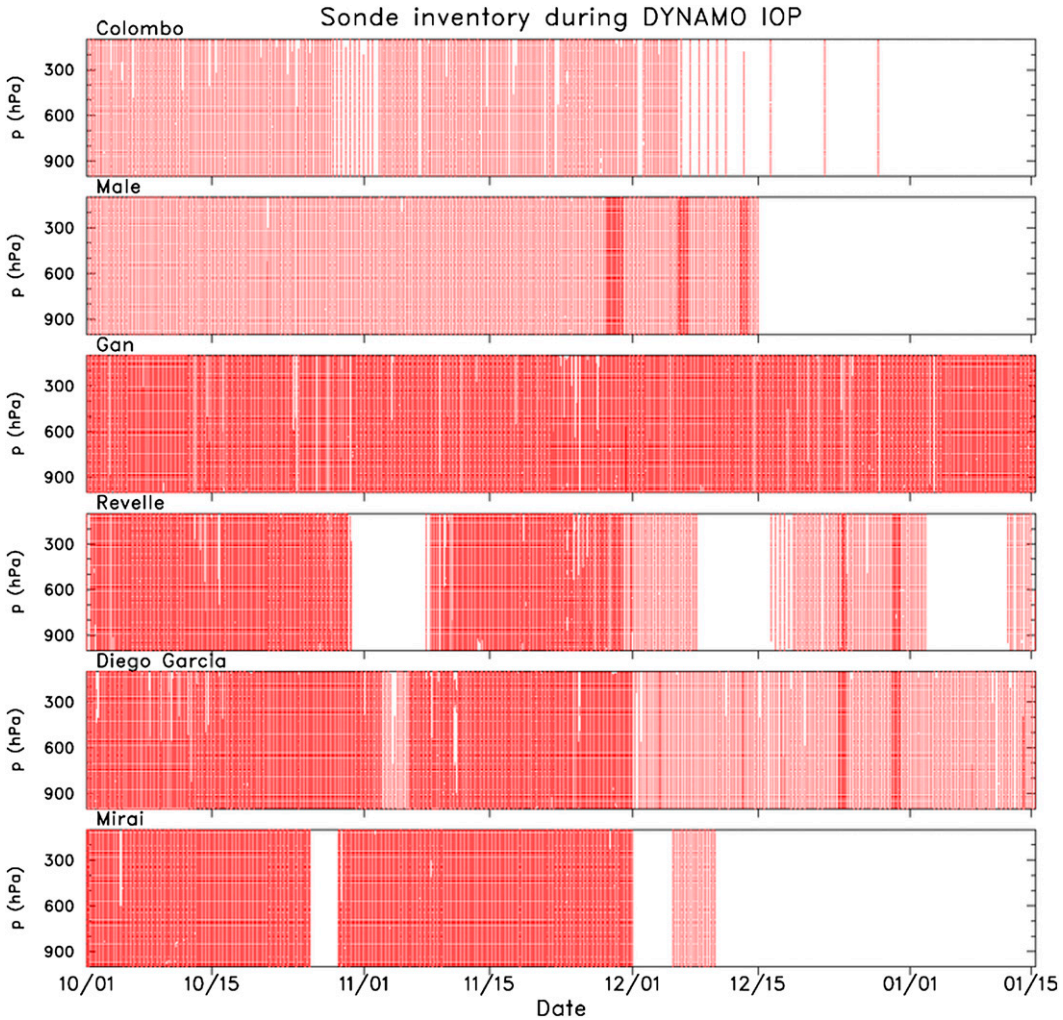

FIG. 2. Visual sounding inventory of upper-air data for six core sites based on L4 data (i.e., 5-hPa interpolated). Each line of dots represents a successful sonde launch. Larger data gaps at *Revelle* and *Mirai* are the result of ship port calls.

TABLE 2. DYNAMO site information for stations for which hi-res sonde data were collected. Enhanced sites are in boldface. Native resolution refers to the vertical time resolution of the data received at NCAR EOL.

Site	Station ID	Sonde type	Native resolution (s)	No. of soundings	Dates of retrieved data
Ambon	97724	Meisei RS06G	1	363	1 Oct 2011–31 Mar 2012
R/V *Baruna Jaya*	**YEAU**	**Vaisala RS92-SGP**	**2**	**58**	**5 Dec 2011–18 Dec 2011**
Biak	97560	Meisei RS06G	1	347	1 Oct 2011–31 Mar 2012
Colombo	**43466**	**Meisei RS06G**	**1**	**258**	**1 Oct 2011–28 Dec 2011**
Darwin	94120	Vaisala RS92-15	2	397	1 Oct 2011–31 Mar 2012
Diego Garcia	**DRG**	**Vaisala RS92-SGP**	**1**	**679**	**30 Sep 2011–15 Jan 2012**
P3 dropsondes	NOAA3	Vaisala RS92-SGP	0.25	469	9 Nov 2011–13 Dec 2011
Gan	**43599**	**Vaisala RS92-SGP**	**2**	**1250**	**15 Jun 2011–8 Apr 2012**
Guam	91212	VIZ B2	6	297	1 Oct 2011–31 Mar 2012
Jakarata	96749	Meisei RS06G	1	356	1 Oct 2011–31 Mar 2012
Koror	91408	Sippican Mark IIA	1	339	1 Oct 2011–31 Mar 2012
Kupang	97372	Meisei RS06G	1	349	1 Oct 2011–31 Mar 2012
Makassar	97180	Meisei RS06G	1	337	1 Oct 2011–31 Mar 2012
Malé	**43555**	**Vaisala RS92-SGP**	**2**	**323**	**29 Sep 2011–15 Dec 2011**
Manado	97014	Meisei RS06G	1	361	1 Oct 2011–31 Mar 2012
Manus	**92044**	**Vaisala RS92-SGP**	**2**	**1411**	**25 Sep 2011–31 Mar 2012**
Medan	96035	Meisei RS06G	1	364	1 Oct 2011–31 Mar 2012
Merauke	97980	Meisei RS06G	1	364	1 Oct 2011–31 Mar 2012
R/V *Mirai*	**JNSR**	**Vaisala RS92-SGP**	**2**	**518**	**26 Sep 2011–10 Dec 2011**
Nairobi	**63741**	**Vaisala RS92-SGP**	**2**	**198**	**1 Sep 2011–5 Mar 12**
Nauru	91532	Vaisala RS92-SGP	2	337	1 Oct 2011–31 Mar 2012
Padang	96163	Meisei RS06G	1	421	1 Oct 2011–31 Mar 2012
Palu	97072	Meisei RS06G	1	365	1 Oct 2011–31 Mar 2012
Pangkal	96237	Meisei RS06G	1	297	5 Oct 2011–31 Mar 2012
Pontianak	96851	Vaisala RS92-SGP	2	57	3 Dec 2011–1 Jan 2012
Ranai	96147	Modem M2K2DC	1	321	8 Sep 2011–29 Feb 2012
R/V *Revelle*	**KAOU**	**Vaisala RS92-SGP**	**1**	**635**	**30 Aug 2011–10 Feb 2012**
R/V *Sagar Kanya*	**VTJR**	**Vaisala RS92-SGP**	**2**	**71**	**25 Nov 2011–19 Oct 2011**
Seychelles	**63985**	**Vaisala RS92-SGP**	**2**	**320**	**28 Oct 2011–31 Mar 2012**
Singapore	48698	Vaisala RS92-SGP	2	163	1 Oct 2011–21 Dec 2011
		Graw DMF-09	1	202	21 Dec 2011–31 Mar 2012
Sipora		Vaisala RS92-SGP	2	215	29 Nov 2011–1 Jan 12
Surabaya	96935	Meisei RS06G	1	365	1 Oct 2011–31 Mar 2012
Yap	91413	Sippican Mark IIA	1	267	30 Sep 2011–31 Mar 2012

In addition to the 11 enhanced sites, 45 operational sites in the large-scale domain of DYNAMO were identified prior to the experiment as important to providing a broader-scale context for the core DYNAMO observations. An effort was made to obtain hi-res data from these priority sounding sites (PSS) by sending requests to many of the countries involved. While these requests were met with limited success, in the end hi-res data were obtained from 21 of these sites (identified with a black dot in Fig. 1). Station information for sites in which high-vertical-resolution data were collected is listed in Table 2, including dropsondes from 13 National Oceanic and Atmospheric Administration (NOAA) P3 aircraft missions. Two of the sites listed in Table 2, Pontianak and Sipora, represent part of an enhanced sounding network for the Hydrometeorological Array for Interseasonal Variation (ISV)-Monsoon Automonitoring (HARIMAU) project (Yamanaka et al. 2008).

For the remaining 24 PSS without hi-res data (white dots in Fig. 1), an effort was made to obtain a complete record of their Global Telecommunication System (GTS) resolution data by utilizing the University of Wyoming sounding data archive (http://weather.uwyo.edu/upperair/sounding.html). During the field phase of the experiment GTS resolution data were collected for an additional 16 non-PSS in the DYNAMO region (indicated with a gray dot in Fig. 1). Though no special effort was made to ensure a complete data record for the non-PSS, the majority of these sites averaged better than one sounding per day.

Table 3 summarizes the number of soundings collected for each type of site. In total 25 938 upper-air soundings were collected and quality controlled, and are archived at the DYNAMO data archive at the NCAR Earth Observing Laboratory (EOL). Included in this number are ~5000 pilot balloons (pibals), which are winds only, generally in the lowest few kilometers of the troposphere. A map of the pibal sites is shown in Fig. 3. The red dots for the Australian sites in this figure indicate that wind observations taken at these stations were over a much

TABLE 3. Inventory of upper-air sonde data. Note that the 24 sites with pibal data at 0600 and 1800 UTC generally had rawinsonde data at 0000 and 1200 UTC. Low-res signifies low vertical resolution.

Site type	No. of sites	Vertical resolution	No. of soundings
Enhanced	11	1–2 s	5721
P3 dropsondes	1	0.25 s	469
PSS (hi-res)	21	1–6 s	6884
PSS (low-res)	24	15–25 hPa	5078
Non-PSS (low-res)	16	15–25 hPa	2581
Pibal (winds only)	27	30–40 hPa	5205
Total	73		25 938

greater vertical extent (e.g., up to 100 hPa). Typically, pibal observations in the DYNAMO domain were taken at 0600 and 1800 UTC between rawinsonde observations at 0000 and 1200 UTC. Of the total soundings, 13 074 (~50%) are hi-res. In comparison, the TOGA COARE data archive consists of 14 310 soundings of which 11 245 were hi-res.

b. Network performance

Developing a research quality dataset begins with our ability to collect high-quality data. Toward this end, a detailed list of "best sounding" launch practices [see sidebar on sounding data quality assurance in Ciesielski et al. (2012)] was established prior to the experiment to guide station setup and sonde operators. To our knowledge, these guidelines were generally followed at the core sounding sites, which contributed to their overall excellent performance and quality as will be shown. The launch success rate (defined as the ratio of successful launches to those planned) for the 11 enhanced sites is shown in Table 4. Values less than 100% are due to aborted or missed launches for a variety of reasons generally related to weather or instrument issues. Ground system equipment failures during parts of the extended observing period (EOP) caused the lower rates at Nairobi, Kenya (24 November–6 December 2011), and the Republic of Seychelles (1–27 October 2011). The statistics for Gan Island in this table are valid through 8 February 2012 when Department of Energy (DOE) intensive observations (eight soundings per day) ended prematurely due to political unrest in the Maldives. The overall success rate for the six core sites during the SOP is ~98%.

One measure of a successful launch is the vertical extent of the observations (that is to say, the higher the better). Table 4 lists the mean sounding termination (or burst) altitude for the 11 enhanced sounding sites.[1] Except for the R/V *Sagar Kanya*, this level is at or above 75 hPa (~18 km) for all sites. These means are decreased slightly at some sites by inclusion of a small number of soundings (listed in Table 4) that terminated at or below the freezing level (~550 hPa), likely due to icing on the balloon.

Based on the number of soundings taken in DYNAMO along with their excellent coverage in time and height, sounding operations were deemed an extraordinary success, especially considering the remote location of many of the sites. Discussion in subsequent sections will focus on the quality of the sounding data.

c. Other data sources

With the objective of providing reference observations for climate studies, the Global Climate Observing System (GCOS) program is establishing a GCOS Reference Upper Air Network (GRUAN; Immler and Sommer 2011) presently consisting of 15 sites with an ultimate goal of 30–40 sites worldwide (Seidel et al. 2009). To assist in evaluating the quality of the DYNAMO observation, GRUAN Vaisala RS92 (VRS92) data processing was performed on data for three sites (Gan Island, Manus Island, and Nauru Island). An advantage of the GRUAN-processed data is that a comprehensive uncertainty analysis is provided for each observation (Immler et al. 2010).

To evaluate sonde humidity measurements, independent estimates of PW are valuable for determining total-column biases. Independent estimates of PW can come from several sources, including ground-based microwave radiometers (MWR) retrievals (Cady-Pereira et al. 2008), satellite-based microwave (MW) retrievals over the oceans (Wentz 1997), and ground-based GPS estimates over land and on ships (Wang et al. 2007). Ideally the independent measurements should be collocated with the sounding location. Eleven sounding sites (indicated with red station names or numbers in Fig. 1) had collocated GPS data and four of these locations (Gan Island, Manus Island, Darwin Island, and Nauru Island), being ARM-equipped sites, had collocated MWR data. The reported accuracy of GPS retrievals is ~1–2 mm (Liou et al. 2001; Bock et al. 2007; Wang et al. 2007), making them an excellent source for identifying sonde biases (e.g., Wang and Zhang 2008). Cadeddu et al. (2013) reported the uncertainty in MWR PW retrievals to be 0.5 mm with a calibration independent of sonde data. Since MWR observations are not reliable when liquid water is present on the radiometer window, rain-contaminated MWR estimates were removed if their PW value exceeded the sonde PW by 1.5σ, where σ is the sonde PW standard deviation. For comparisons with sonde PW, the two-channel MWR channel radiometer data, available at 1-min resolution, were averaged into 1-h bins.

The GPS PW came from a variety of sources. For the 2-h PW data from Diego Garcia; Guam; Singapore;

[1] The level at which a balloon bursts is a primarily a function of balloon size, amount of gas used to fill the balloon, and weather conditions. These factors varied from site to site.

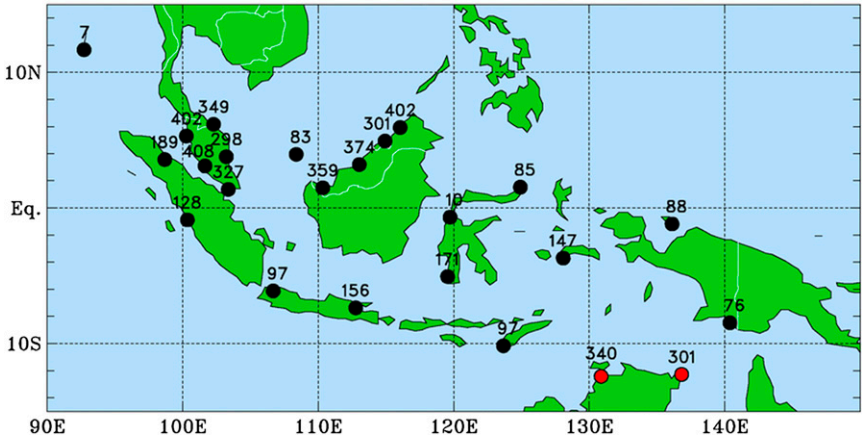

FIG. 3. DYNAMO pibal network with the number of pibal (wind only) soundings indicated next to each site. Wind data from these soundings are generally available only in the lowest few kilometers of the atmosphere. Red dots at Australian sites indicate that winds at these sites extended through the depth of the troposphere.

Jakarta, Indonesia; and Seychelles processed by NCAR EOL, the zenith total delay (ZTD) data are from the International Global Navigation Satellite Systems (GNSS) Service (IGS) solutions and the PW is derived using the algorithm described in Wang et al. (2007). The 30-min PW data at Gan, Manus, Nauru, and Darwin were processed by the University Corporation for Atmospheric Research (UCAR) using the network method (Ware et al. 2000). Data for the two moving platforms, the R/V *Mirai* and the R/V *Revelle*, were processed separately by the Japan Agency for Marine-Earth Science and Technology (JAMSTEC; at 1-min intervals) and UCAR (at 30-min intervals) using methods described by Fujita et al. 2008 and Rocken et al. (2005), respectively. Each of these four GPS processing sources utilized state-of-the art analysis methods similar to those described by Steigenberger et al. (2006). This includes the use of absolute phase center models, modern tropospheric mapping functions, and the utilization of data below 10° elevation. For compatibility with the sonde and MWR measurements, the GPS data, being at 1-min, 30-min, or 2-h resolution depending on the site, were averaged to 1-h bins.

Satellite estimates of PW were obtained from the Microwave Integrated Retrieval System (MIRS) PW product for the period 1 October 2011–14 February 2012. This operational NOAA product is available on an hourly basis at ~0.1° resolution over all surfaces and in all weather conditions. Details of the MIRS retrieval algorithm, which blends microwave PW estimates from several satellites, and some performance statistics can be found in Kidder and Jones (2007) and Boukabara et al. (2010).

Quality-controlled soundings were used to evaluate relative humidity analyses from two numerical weather prediction (NWP) centers: European Centre for Medium-Range Weather Forecasts (ECMWF) and the National

TABLE 4. Additional information for enhanced sonde sites. Launch success rate is defined as percent of successful launches to number planned. Premature termination means sonde did not ascend above freezing level (~550 hPa). Statistics for Gan are only through 8 Feb 2012, when DOE operations ended at this site.

Site	No. of soundings	Launch success rate (%)	Missed launches	Mean burst altitude (hPa)	No. of premature terminations
R/V *Baruna Jaya*	58	100.0	0	41.2	0
Colombo	258	93.8	17	66.2	0
Diego Garcia	679	98.4	11	69.9	13
Gan	1066	97.8	24	60.5	24
Malé	323	100.0	0	53.8	0
Manus	1411	93.4	99	62.8	46
R/V *Mirai*	518	100.0	0	43.0	3
Nairobi	198	71.6	78	32.4	3
R/V *Revelle*	635	98.4	10	72.9	13
R/V *Sagar Kanya*	71	97.3	2	136.0	0
Seychelles	320	85.8	53	33.2	2

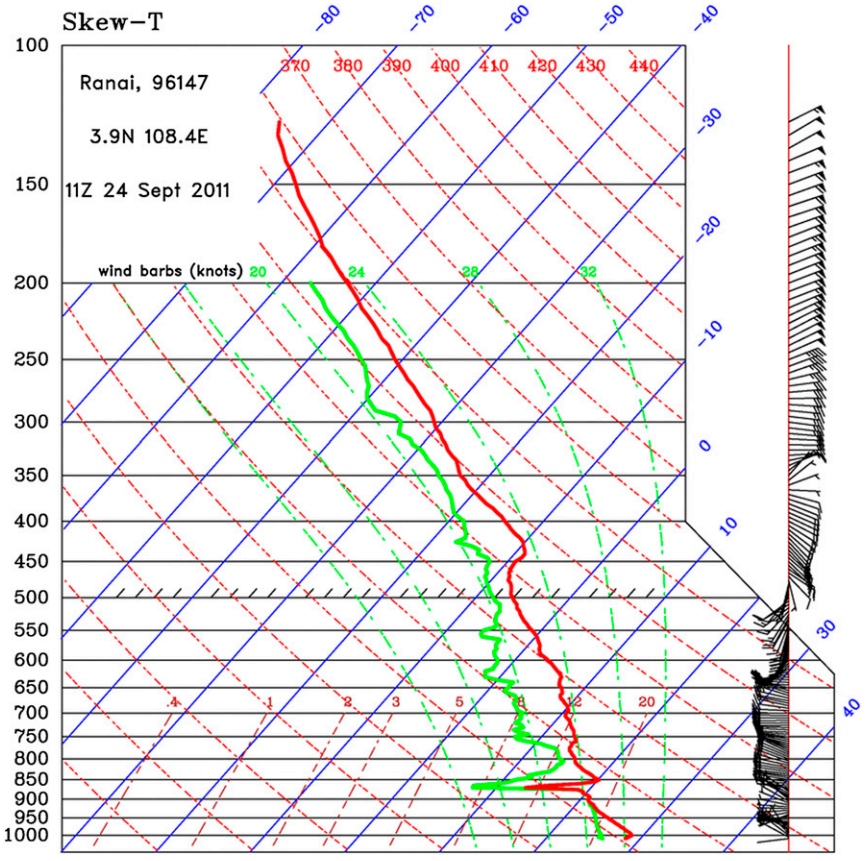

FIG. 4. Skew *T* for Ranai at 1100 UTC 24 Sep 2011 showing "wetbulbing effect" near 850 hPa. This effect results when a sonde is not properly ventilated, such that wetting of the thermistor in the cloud layer results in excessive cooling by evaporation or sublimation once the sonde exits the cloud.

Centers for Environmental Prediction (NCEP). Operational data from ECMWF were at 0.25° horizontal resolution, 20 vertical levels from the surface to 20 hPa, whereas data from the NCEP Global Forecast System (GFS) were at 1° horizontal resolution, 32 vertical levels from the surface to 20 hPa. Both analyses were available at 6-hourly intervals for the period 1 October–31 December 2011. During the field phase of the experiment, a major effort was undertaken to ensure the real-time transmission of the sonde data onto the GTS for dissemination to the operational NWP centers. Preliminary estimates indicate that ~95% of the soundings from the core sounding network were received at the centers (J. Whiting 2012, personal communication) to be used in their data assimilation schemes.

3. Quality control procedures

This section describes the general processing of the hi-res sonde data, which follows the schemes outlined in Loehrer et al. (1996) and Ciesielski et al. (2012). While no corrections are applied to GTS resolution data due to the lack of information describing sonde type and age, sonde ascent rate, etc., gross limit checks and visual inspection were used to flag questionable GTS data.

The first step in processing hi-res sonde datasets was to convert the raw level 0 (L0) sounding data from the various data formats created by the different data systems into a single, easily utilized format that we refer to as level 1 (L1) processing. In DYNAMO the hi-res sonde data came from six different sonde types (see Table 2) and 12 unique data formats. All hi-res soundings (level 1 through level 3) contain the basic fields (pressure, height, temperature, relative humidity, and winds) as well as ancillary fields (e.g., sonde ascent rate and geolocation information) as a function of time. Header lines in each sounding include the exact time of the sonde launch and the sonde serial number, which provide information on the manufacture date, which can prove helpful in developing corrections.

These efforts were followed by level 2 (L2) processing in which the hi-res soundings were passed through

TABLE 5. Dataset naming convention with brief description of processing performed at each level.

Level	Description
L0	Raw, unprocessed hi-res data in original formats
L1	Initial hi-res data: uniform, easily readable format
L2	Preliminary hi-res data: processed with automated and visual QC
L3	Final hi-res data: corrected for biases and errors if necessary
L4	Uniform vertical resolution data created from hi-res datasets and GTS resolution soundings processed with objective QC checks and visual inspection

a series of automated QC algorithms (Loehrer et al. 1996) and visual inspection to systematically detect suspicious data values. Because of the unique data format produced by the two ISS, L2 processing of data from these sites used NCAR's Atmospheric Sounding Processing Environment (ASPEN) software (see http://www.eol.ucar.edu/isf/facilities/software/aspen/aspen.html).

In level 3 (L3) processing, errors and biases in the data were identified and corrected, if possible. With recent improvements in radiosonde technology—in particular, GPS-derived winds and ground station software—biases in temperature, pressure, and winds are generally quite small (Nash et al. 2011) and their measurements are of suitable quality for both weather and climate research. However, as will be seen in the next section, special care must be taken in analyzing soundings obtained from ships, which may contain errors in the boundary layer temperature and humidity fields due to contamination from the ship structure (Yoneyama et al. 2002).[2] L3 processing resulted in the final high-resolution datasets to which corrections have been applied whenever such corrections were deemed necessary or possible.

While sonde manufacturers are continually striving to improve the accuracy of humidity sensors, water vapor continues to be the most problematic variable measured by upper-air sondes (Miloshevich et al. 2009; Nash et al. 2011). Since one of the primary goals of the experiment was to investigate the moistening processes during the initiation phase of the MJO, a special effort was made to minimize humidity errors. While use of well-calibrated surface data can provide an indication of low-level sonde biases, independent estimates of PW, as described in section 2, are valuable for determining total-column biases. The next section describes the errors identified

[2] Of course, soundings from islands and atolls also have local effects that make the data at low levels unrepresentative of the surrounding ocean. Depending on the application, this situation must be considered when evaluating the sounding data.

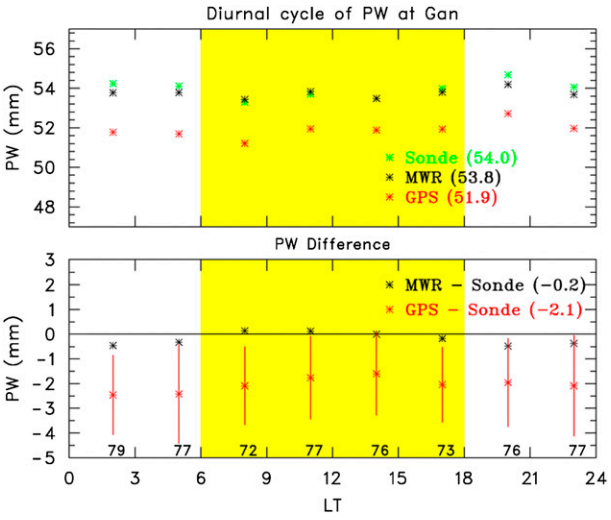

FIG. 5. (top) Diurnal cycle of PW (mm) at Gan covering the period from 1 Oct to 14 Jan 2012 for three independent estimates (sonde—green, MWR—black, GPS—red). Number in parentheses represents the period mean. (bottom) Diurnal cycle of PW difference: GPS minus sonde (red) and MWR minus sonde (black). Vertical red lines show std dev of GPS minus sonde PW difference. Number along the bottom of the plot indicates the number of comparison observations. Yellow shading denotes daylight hours.

in the hi-res DYNAMO sounding dataset and the details of their corrections.

Finally, in level 4 (L4) processing a more "user friendly" version of the sounding dataset was created with QC flags assigned to each variable, providing a measure of the data's reliability. L4 processing was performed on sites with both GTS resolution and hi-res data, where L3 hi-res data were vertically interpolated to create values at uniform pressure intervals. Suspicious data were identified through application of both an objective QC test as in Loehrer et al. (1996) and a subjective adjustment of QC flags by visual inspection (Ciesielski et al. 2012). While tedious, visual inspection was necessary to ensure a research-quality dataset, since subtle errors in sonde data (e.g., superadiabatic layers near cloud top due to wet bulbing effects as seen in Fig. 4, layers of suspicious wind shear, boundary layer abnormalities, etc.) are often difficult to identify with objective procedures. By flagging suspect data values, the reliable data are easily retrievable with the users deciding what level of quality is acceptable for their analyses.

This second pass of QC checks and visual inspection, beyond those in L2, ensured the veracity of the L3 corrections and provided yet another filter for identifying suspicious values. Note that the QC checks and visual inspection in L2 and L4 processing did not change any data values, only data quality flags. Additional details on

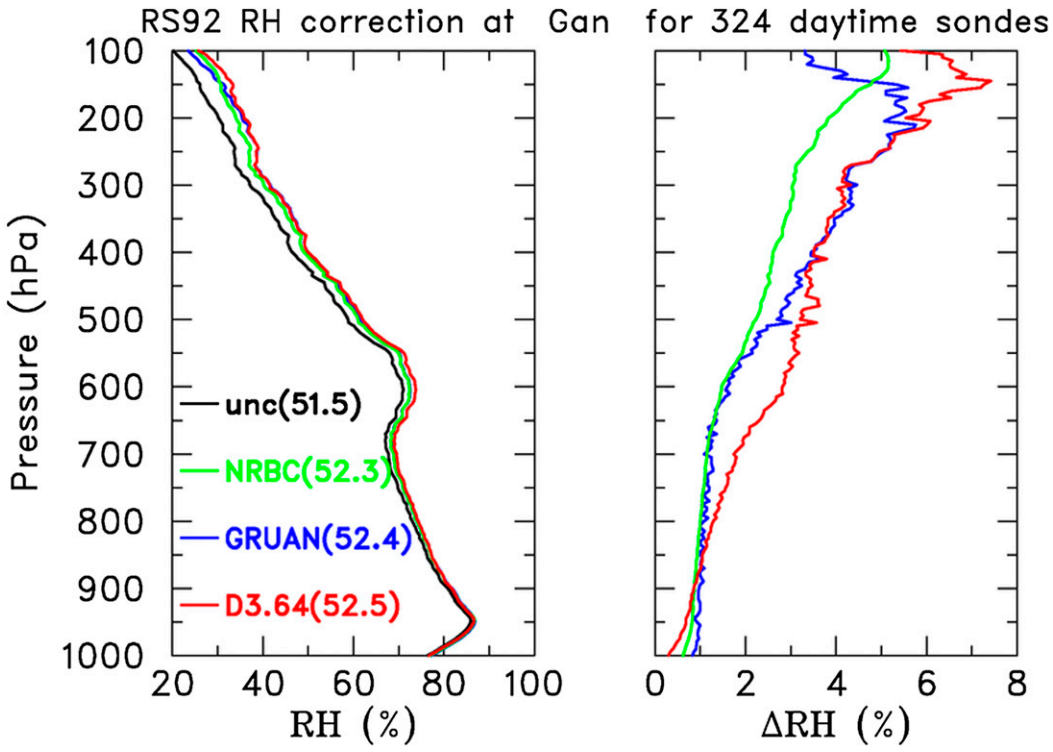

FIG. 6. Mean vertical profiles of RH (%) with respect to water at Gan for daytime soundings during the 1 Oct–31 Dec 2011 period: (left) uncorrected RH (black), GRUAN-corrected (blue), NRBC-corrected (green), D3.64-corrected (red); (right) difference between corrected and uncorrected profiles. Mean PWs are listed in parentheses.

interpolating the data to uniform pressure intervals, objective tests for assigning QC flags, definition of QC flags, and the visual editor used to expedite this processing can be found online (www.eol.ucar.edu/projects/sondeqc/).

A summary of the various sounding dataset categories is provided in Table 5. Datasets are referenced by both a level number and a version number within each level. For example, L3.0 signifies level 3 version 0 of that dataset. If additional corrections are needed in the future, then the version number will be incremented accordingly (e.g., L3.1). For sites with hi-res data, both L3 and L4 datasets are available from the DYNAMO data archive. L1 and L2 datasets are available upon request to EOL. All hi-res datasets are available in EOL sounding composite (ESC) format, which is a simple-to-read ASCII format. Level 4 datasets are also provided in a simple ASCII format.

4. Identification of errors and their correction

In this section we describe the errors identified in the L2 hi-res soundings and the details of their corrections to produce a L3 dataset. These corrections include humidity adjustments to Vaisala, Meisei, and Modem sondes; correction of low-level thermodynamic fields in the Graw sondes at Singapore and in ship soundings due to deck heating/cooling effects; baseline (or surface data) corrections in Manus, Malé, and *Revelle* sondes; and correction of artificial dry spikes in slow-ascent soundings.

a. Humidity corrections

Of the 15 sites in DYNAMO using VRS92 upsondes, four of the sites (Malé, Gan, Manus, and *Mirai*) were running Digicora 3.64 (D3.64) ground station software. This software version, introduced by Vaisala in 2010, provides humidity corrections for the daytime soundings, which include a solar radiation dry bias (SRDB) correction and a time-lag correction for the slow response of the humidity sensor at cold temperatures. Only time-lag corrections are applied at night. Because of the proprietary nature of the Digicora software, information on the details of these corrections is not available. The SRDB, being the largest of the corrections, was first quantified in a study by Vömel et al. (2007), who found relative humidity (RH) dry biases of ~9% near the surface increasing to >50% near 100 hPa. Changes to the coating of the VRS92 humidity sensor in 2006 and 2008 (Vaisala 2011) have reduced, but not eliminated, these biases.

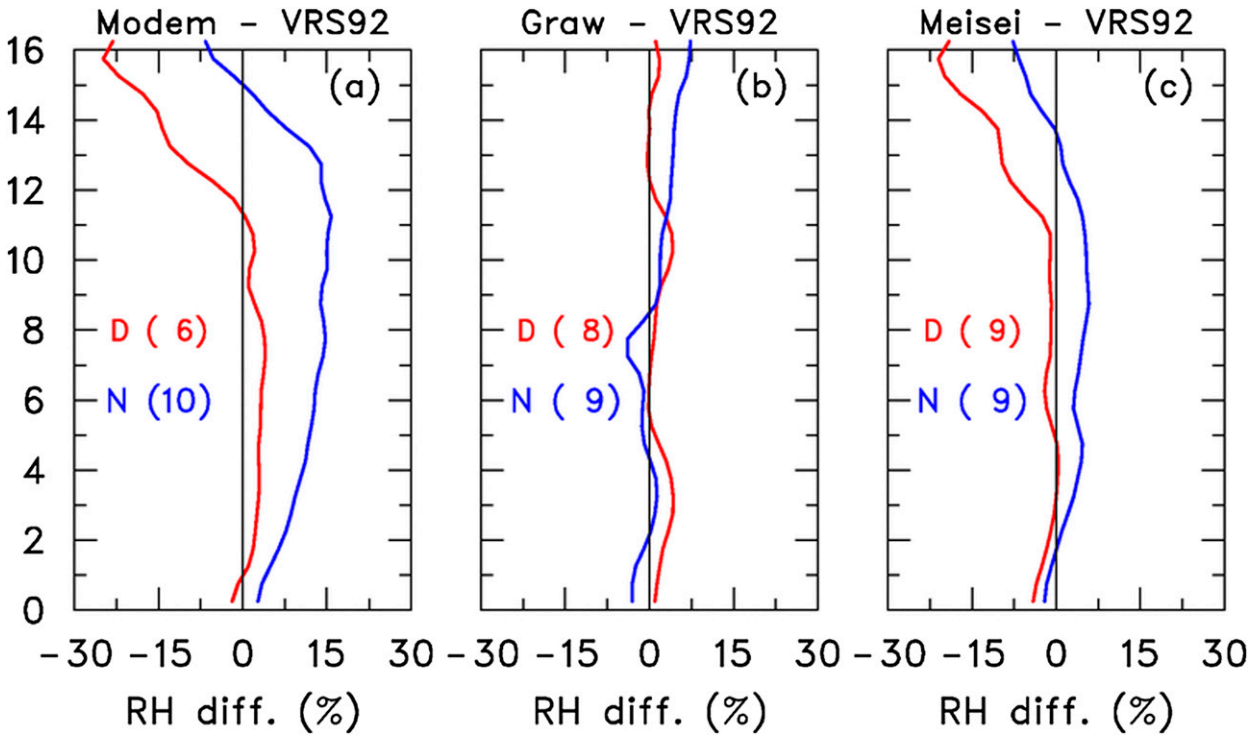

FIG. 7. Vertical profiles of mean RH difference (%) between VRS92 and (a) Modem, (b) Graw, and (c) Meisei sondes for day (red) and nighttime (blue) launches based on data from the WMO 2010 intercomparison study. A positive (negative) difference indicates a moist (dry) bias in the sonde relative to the Vaisala sonde. Numbers in parentheses indicate the number of intercomparison soundings that went into computing mean differences.

To evaluate the moisture measurements from these systems, Fig. 5 shows a comparison over the diurnal cycle for Gan between sonde PW and two independent estimates: a GPS and an ARM-deployed MWR. This analysis considers only times when all three instruments had reliable PW estimates (e.g., sonde moisture data must be present from the surface up to 200 hPa and rain-contaminated MWR estimates were removed). Differences between the sonde and MWR PW are less than 0.5 mm at individual hours and only 0.2 mm in the mean. Similar agreement between sonde and MWR PW was found at Manus (not shown), which also had MWR and GPS estimates of PW. This excellent agreement gives us confidence that the humidity measurements provided by the sites using VRS92 sondes with D3.64 software *need no further humidity corrections.* While a slight (~0.4 mm or <1%) moist bias is seen in the nighttime sonde data relative to the MWR, previous studies (Miloshevich et al. 2009; Cady-Pereira et al. 2008; Bock and Nuret 2009) have noted a more pronounced nighttime moist bias (up to 3%) in VRS92 sondes. However, a statistically significant nighttime moist bias was not consistently observed in the DYNAMO VRS92 sondes to warrant additional corrections.

For reasons unclear at this time, the GPS PW values at both Gan and Manus are systematically ~2 mm lower than the other estimates. Standard deviation estimates of the GPS minus sonde PW difference (bottom panel of Fig. 5) show that the GPS PW biases are indeed significant. At other sites in the DYNAMO domain (seen later in Fig. 14), there is a dry bias in the GPS PW from each of the four different GPS data sources, although the magnitude of the bias varies from site to site. The source of this bias is unclear, but it is consistent with results reported by Thomas et al. (2011), who quantified the impact of the current state-of-the-art GPS analysis techniques and found that they underestimate PW by ~1.8 mm in high latitude and dry atmospheric conditions. These modern analysis techniques were used to compute PW for this current study and could provide a potential explanation for the GPS biases observed here, but they may not be applicable to earlier studies where GPS biases were found (e.g., Wang et al. 2007). Despite the dry bias in the GPS observations, it is noteworthy that all three estimates of PW in Fig. 5 show a slight but similar diurnal trend with nighttime means ~1.5 mm higher than daytime means.

Eleven sites in DYNAMO used VRS92 sondes (see Table 2) that did not have software that included a SRDB correction. For soundings from these non-D3.64 sites, we used a recent correction scheme developed by Wang et al. (2013) that is referred to as the NCAR radiation bias

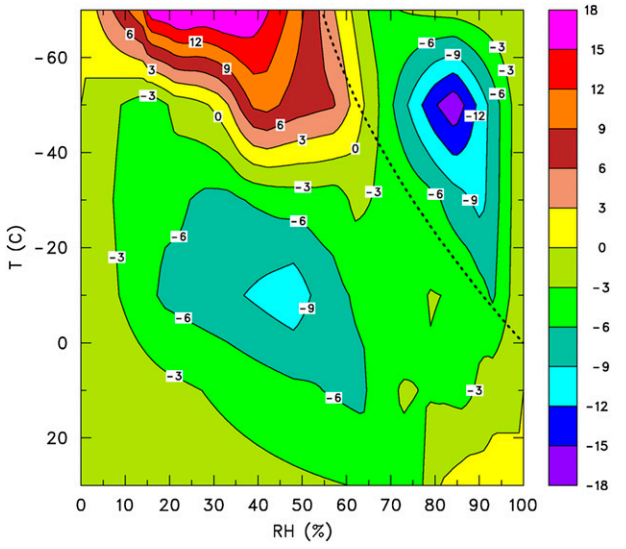

FIG. 8. RH bias correction (%, contour increment of 3%) for Modem sondes covering the full range of temperatures created by matching the Modem and VRS92 CDFs for eight dual launches. Axes are temperature and RH as observed by Modem sondes. Light dotted line represents saturation with respect to ice.

correction (NRBC). Designed to correct the SRDB and being a function of pressure, temperature, RH, and solar elevation angle, this easy-to-use algorithm is based on the more complicated GRUAN correction. As in the D3.64 software, the GRUAN algorithm also includes an SRDB and time-lag correction, although the exact nature and implementation of these corrections are undoubtedly different between algorithms. In addition, GRUAN applies an RH calibration correction which increases RH slowly above the 0°C level to a maximum of ~3% near 200 hPa. Figure 6 shows a comparison of the mean vertical profiles of RH (right panel) for the various corrections of Gan daytime soundings. Differences in RH below 700 hPa among the three corrections (left panel) are quite small (less than 1% at any given level). Since ~80% of the moisture for PW comes from the surface to 700 hPa layer, consequently mean PWs computed with the corrected data show excellent agreement (ranging from 52.3 to 52.5 mm) and lend confidence for using the NRBC in DYNAMO. Application of NRBC increases PW ~0.8 mm in the daytime soundings. The difference between the GRUAN and NRBC corrections above the freezing level (~550 hPa) results primarily from GRUAN's calibration correction (R. Dirksen 2013, personal communication), since the time-lag correction is of consequence only above 200 hPa but even then it generally changes the mean RH by less than 1%. Because of its proprietary nature, the causes of the larger D3.64 corrections, particularly between 500 and 700 hPa, are unknown. Since the calibration and time-lag corrections are less robust (i.e., biases within the measurement uncertainty; Vömel et al. 2007) and result in insignificant changes to PW (≤0.2 mm), they are not applied to the non-D3.64 VRS92 sondes.

To determine the need for humidity corrections in Meisei, Graw, and Modem sondes used at several sites in DYNAMO (see Table 2), data from the Eighth World Meteorological Organization (WMO) Intercomparison of High Quality Radiosonde Systems held in Yangjiang, China, in July 2010, were used.[3] In this study 11 operational and two reference sondes were examined in 72 intercomparison launches conducted in a variety of weather conditions and through the course of the 24-h day.

Because of the small biases found in VRS92 D3.64 sondes in DYNAMO and their excellent agreement to the reference cryogenic frost point hygrometer (CFH) sondes in the WMO study (Nash et al. 2011), the VRS92 sondes are used here as a reference. Figure 7 shows the comparison of RH profiles for day and nighttime dual launches for three sonde types compared to the VRS92. The biases in the Graw sondes were within the stated accuracy of the RH measurements of the VRS92 and Graw sensors (~5%); thus, no bias correction is needed for this sonde type. On the other hand, the size of the biases in the Modem and Meisei sondes indicates that application of a correction would be beneficial.

To correct the Modem sondes at Ranai, Indonesia, the cumulative distribution function (CDF) matching method was used. This method attempts to match the statistics of the problem sonde (in this case, Modem) to those of the reliable sonde (i.e., VRS92). Details of this method and examples of its application can be found in Nuret et al. (2008) and Ciesielski et al. (2010). Since the sondes at Ranai were released near 0700 and 1900 LT, WMO intercomparison sonde launches within 2 h of these times were used. With these criteria, eight dual Modem–Vaisala twilight sondes were used in constructing the correction table shown in Fig. 8. This table shows that the MODEM sondes have a moist bias throughout most of the troposphere. Only at colder temperatures (<−50°C) and drier conditions (RH < 60%) do the Modem sondes exhibit a dry bias relative to the Vaisala sondes. Figure 9 shows the magnitude of the correction on the mean RH and specific humidity q profiles. As one might expect based on Fig. 8, the correction results in a mean PW decrease of 1.8 mm (~3%) with a drying effect between 950 and 200 hPa and moistening above this level. The peak drying in terms of q

[3] The same Graw, Meisei, Modem, and Vaisala sonde models were used in both the WMO sonde intercomparison study and DYNAMO.

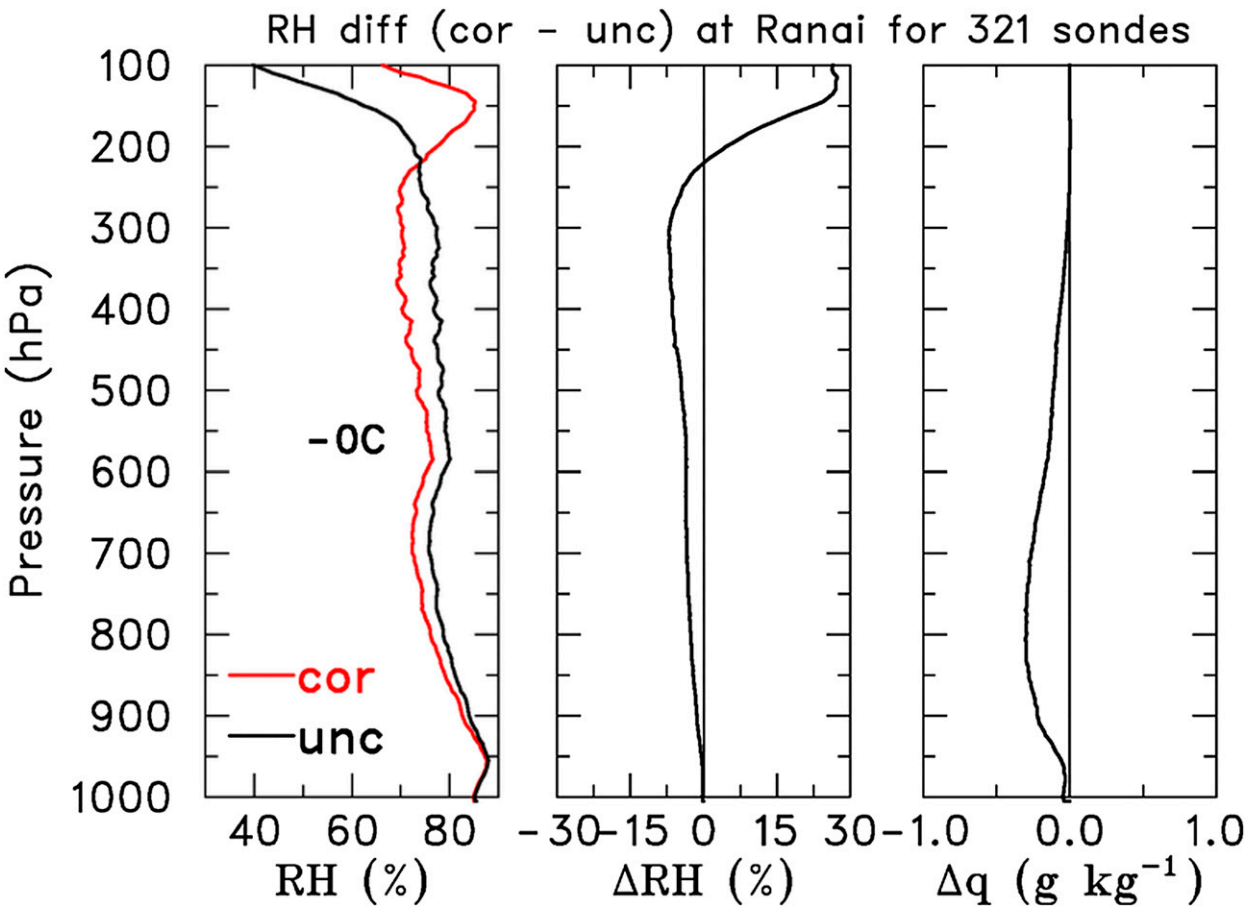

FIG. 9. Magnitude of humidity corrections at Ranai: (left) mean corrected (red) and uncorrected RH with respect to ice for $T < 0°C$ (black) profiles, (middle) RH difference due to correction, and (right) q difference due to correction.

occurs around 800 hPa, being ~0.4 g kg^{-1}. The corrected mean profile closely resembles those from nearby sites (e.g., see the Singapore profile shown later in Fig. 19) with upper-level RHs approaching 85%.

As seen in Table 2, the Singapore site switched from Vaisala to Graw sondes on 21 December 2011. While this switch did not result in notable humidity biases per se, a change in the launch procedure[4] at this time resulted in suspicious low-level thermodynamic fields. In fact, questionable temperature T and dewpoint temperature T_d data were observed at low levels (up to 40 s after launch or the lowest 15–20 hPa) in ~90% of the Graw sondes. Because the corrupted data can readily be identified by large, unrealistic gradients in the low-level T and T_d fields (Fig. 10), a simple procedure was developed to correct these data. A visual sounding editor was used to identify questionable data values in the 5-hPa interpolated sounding (L4) dataset. In most cases the surface data, which comes from an independent data source, were of good quality. In this case, new data were generated by linearly interpolating between the surface value and good-quality data immediately above the questionable data. In the few cases where the surface values were suspicious, a one-sided second-order derivative was computed using good low-level L4 data. This gradient was then used to extrapolate corrected values down to the surface. These corrections were made in both the L3 (native resolution) and L4 datasets. An example of uncorrected and corrected low-level T and T_d profiles is shown in Fig. 10.

As shown in Fig. 7c, the Meisei RS06G sondes used in the WMO intercomparison study had humidity biases relative to the reliable VRS92 sondes, indicating that soundings from the 13 sites using such Meisei sondes in DYNAMO need correcting. The humidity corrections of the Meisei sondes, carried out at JAMSTEC, included procedures for removing 1) a discontinuity in RH at 0°C level due to deficiencies in Meisei's software (Sugidachi and Fujiwara 2013) and 2) sonde RH biases using a CDF

[4] Graw sondes were launched from inside a building that was not acclimated to outside ambient conditions.

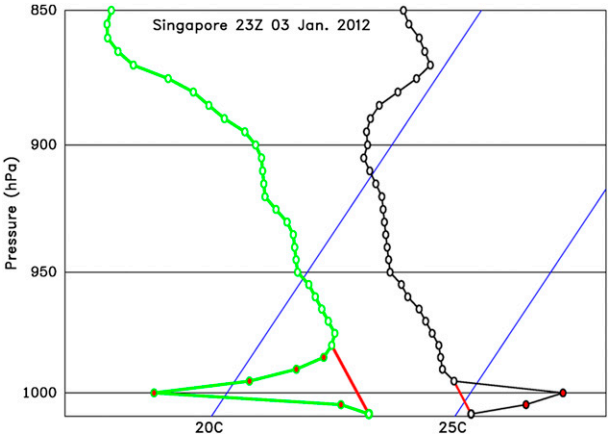

FIG. 10. Example of low-level uncorrected 5-hPa sonde data at Singapore at 2300 UTC 3 Jan 2012 plotted on a skew T diagram, where the black curve is T and the green curve is T_d. Red circles indicate data values identified as bad data. Red lines show linear interpolation using the good data.

matching method based on 33 intercomparison launches (21 daytime and 12 nighttime) of VRS92 and Meisei sondes conducted on *Mirai* cruises during DYNAMO. A daytime correction table was applied to sondes launched from the local sunrise to sunset times; a nighttime correction table was used for other local hours. A comparison of uncorrected and corrected soundings at Colombo shows the impact of the corrections (Fig. 11). In the mean, the correction acts to moisten soundings slightly below 800 hPa and to dry them in a deep layer above this level with more midlevel drying in the nighttime soundings, as suggested by Fig. 7c. Because of the vertical structure of the correction at Colombo, its mean PW decreased 0.4 mm, while convective available potential energy (CAPE) and convective inhibition (CIN) increased 266 and 19 J kg^{-1}, respectively.

While no intercomparison datasets were available to correct the older model Sippican and VIZ sondes used at three western Pacific sites, Wang and Zhang (2008) showed that Sippican sondes have little bias at higher PW values such as observed in this region. A comparison of the EOP mean PW for the VIZ sondes at Guam reveals that the sonde PW is 1.6 mm higher than the GPS PW (Fig. 14, later). While this difference is within the uncertainty of the instruments, the magnitude of the GPS dry bias relative to the sonde data is similar to what is seen at other DYNAMO sites (e.g., see the Gan comparison in Fig. 5).

b. Baseline corrections

The standard WMO practice is to use surface data from a well-calibrated instrument collocated with the sonde launch site as the bottom point of the sounding. These sonde-independent observations can prove useful for identifying low-level biases in the sonde data as demonstrated in TOGA COARE data, where Wang et al. (2002) found large differences between surface and boundary layer q, indicating a sonde dry bias. During the field phase of the experiment, monitoring of the low-level moisture gradient[5] was conducted using GTS resolution data. In this manner, the low-level moisture gradient at Manus was found to be suspiciously negative in the mean; that is, q increased with height in the lowest levels. A negative gradient was not observed at any other sites in the DYNAMO domain. This led to an extensive investigation of the Manus soundings and surface data in which Long and Holdridge (2012) determined that surface data from the automated weather station (AWS) humidity sensor, which was being used to baseline the Manus sounding, had an RH dry bias of about 5%. Furthermore, their report recommended that the surface observations at Manus be switched to those from a nearby SMET system that included a Vaisala HMP45 combined T/RH probe in a forced air enclosure.

Since the 1-min SMET values were available for the entire DYNAMO EOP, the AWS surface T and RH values were replaced with those from the SMET system using the 1-min values closest to the time of launch. Figure 12 shows the diurnal cycle of the q difference δq between the surface and the boundary layer mean, computed with AWS (top) and SMET data (bottom). Using SMET data the mean low-level δq is now positive at all hours of the day. The small mean moisture gradients observed at night even using SMET data are related to the frequent (81% of the time) formation of shallow-surface temperature inversions.

Issues with baseline errors were also observed at Malé and the *Revelle*. To resolve the problems at Malé, AWS values, which exhibited a modest dry bias, were recalibrated using a highly accurate Vaisala HMP155 temperature/humidity probe. These improved surface values were then used to baseline the Malé soundings. At the *Revelle*, a mismatch in the level of the surface observations (19 m) and where the sondes were released (2 m) led to a disparity between the surface and 2-m sonde values, which resulted in several unphysical-looking near-surface thermodynamic profiles. Because of this and the frequent contamination of low-level sonde data by deck heating/cooling effects, the SMET values were replaced by sonde data interpolated to the height of the SMET

[5] The low-level moisture gradient was computed as q at the surface minus q at the first point above the surface. A negative gradient indicates q increases with height.

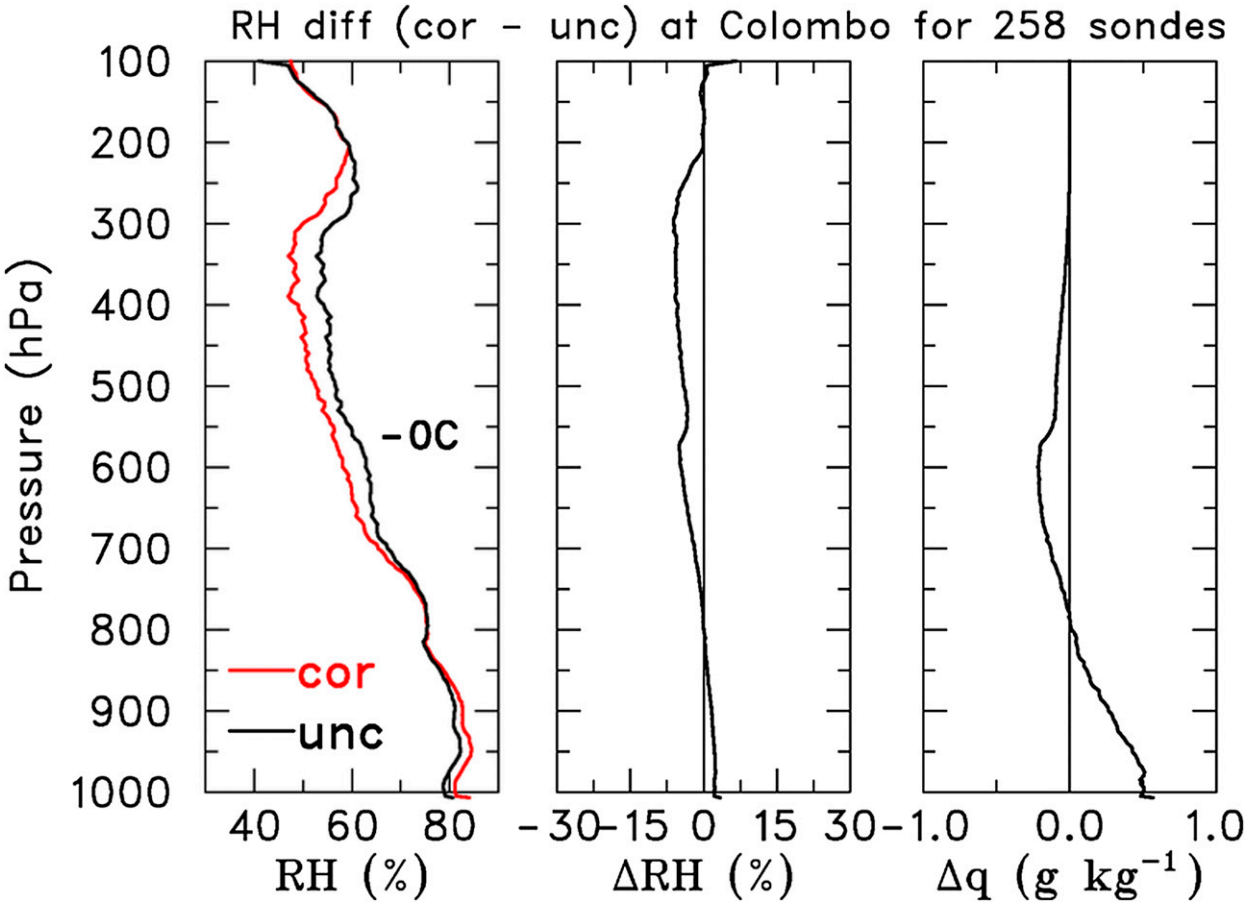

FIG. 11. Magnitude of humidity corrections at Colombo: (left) mean corrected (red) and uncorrected RH with respect to ice for $T < 0°C$ (black) profiles, (middle) RH difference due to correction, and (right) q difference due to correction.

instrument (19 m) with sonde data below this level eliminated in the L3 product.

c. *Ship deck heating/cooling corrections*

As shown in Yoneyama et al. (2002), low-level thermodynamic fields from ship soundings can be distorted under certain conditions by the deck heating and cooling effects. The magnitude of the distortion is a function of ship size, wind speed, and time of day, with larger impacts occurring for larger ships, weaker winds, and during daylight hours. In their analyses of sondes launched on the R/V *Mirai* (128 m; 8700 t), affected data were determined to be restricted to the lowest 40 m of the sounding profile. To remove contaminated data, a simple procedure was designed that linearly extrapolates good data above 50 m down to the surface. This procedure, based on a comparison of regular ship soundings to those taken from a small boat measuring unaffected upwind conditions (Yoneyama et al. 2002), was applied to soundings from the R/Vs *Mirai*, *Baruna Jaya*, and *Sagar Kanya*, which exhibited contaminated data.[6] The distortion of low-level fields on the R/V *Revelle* was more vertically limited due to its smaller size (83 m; 2200 t) such that eliminating the data below 19 m, as described above, was sufficient to remove these effects. Also, a small percentage of the *Revelle* soundings had temperature and humidity spikes, generally 5–10 s into the flight, likely caused by the sonde passing through the ship's smoke plume. The spikes were removed by setting the data values in the affected layers to missing. Additional details on these and other corrections in the R/V *Revelle* soundings are available in Young et al. (2013).

d. *Slow-ascent soundings*

A small percentage of the hi-res Vaisala soundings (~5%) were classified as slow-ascent sondes (ascent

[6] A similar study conducted from the R/V *Baruna Jaya* during DYNAMO confirmed the reasonableness of this procedure for application to DYNAMO ship soundings.

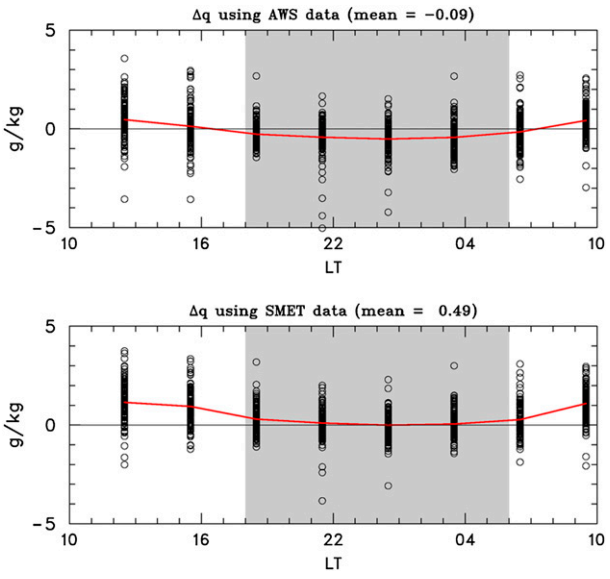

FIG. 12. Diurnal cycle of $\Delta q = q_{sfc} - q_{bl}$, where q_{sfc} is surface q and q_{bl} is the boundary layer mean computed from hi-res Manus sonde data: (top) computed using AWS surface data and (bottom) computed using SMET data. Circles show values at individual times and the red line shows the mean diurnal cycle. Overall means are listed at the top of each plot. Gray shading indicates nighttime hours.

rates $< 3\,\mathrm{m\,s^{-1}}$) which may contain problematic RH profiles containing artificial dry spikes. To eliminate problems with sensor icing, VRS92 sondes are equipped with dual-heated RH sensors that are alternately heated[7], while the nonheated sensor measures the ambient RH (Miloshevich et al. 2009). If the sensors are not adequately ventilated due to a slow ascent resulting from either underfilling of the balloon or icing on the balloon, then the temperature gradient surrounding the heated sensor will not have sufficient time to dissipate, resulting in artificially low RH measurements. An example of these artificial dry spikes in a slow-ascent sounding from the R/V *Mirai* is shown in Fig. 13.

To mitigate this problem, the processing of slow-ascent sondes at the two ISS sites included application of a special filtering within ASPEN to minimize the dry spikes. At other sites, L2 processing marked layers with rapid RH fluctuations as suspicious data. This information was then used in the L4 processing, such that soundings with these layers of suspicious data and slow ascent rates were given special attention. In this manner, L4 visual inspection of these layers with rapid RH fluctuations marked the QC flags for the low RH values as bad and the high RH values as good. For the enhanced sites using VRS92 sondes, ~15% of the slow-ascent sondes exhibited dry spikes, or <1% of all soundings.

5. Assessment of moisture products

This section further examines the corrected sonde humidity data and its impact on various convective parameters. Then, having established the reliability of the corrected sonde moisture data, we use it to evaluate the MIRS satellite-based PW product and moisture fields from the ECMWF and NCEP GFS model operational analyses for the DYNAMO period.

a. Further evaluation of sonde humidity

Having demonstrated the accuracy of the sonde humidity data at a few key sites through comparison with independent estimates, Fig. 14 extends this analysis with similar comparisons for several sites in the larger DYNAMO domain that had collocated, independent estimates of PW. The PW means shown in this figure include only times during the EOP when estimates from all sources were available at a given site. Rain-contaminated MWR estimates were eliminated from the comparison. To ensure the sensors are sampling similar volumes of the atmosphere, Wang et al. (2007) recommend sonde and GPS comparisons only when the GPS sensor is within 50 km of the sonde launch site and their elevation difference is less than 100 m. To provide more accurate comparisons at sites with elevation differences >10 m, sonde PW was computed starting at the elevation of the GPS sensor. This affected three sites—Singapore, Jakarta, and Seychelles—which had sensor height differences of 44, 129, and 537 m, respectively, with the GPS sensor being higher in all cases.

At the four ARM sites with MWR estimates of PW, the sonde minus MWR PW differences ranged from −0.2 to +0.5 mm, lending confidence in the reliability of these estimates. At all sites the GPS PW exhibits a dry bias relative to the sonde ranging from −0.1 to −2.7 mm. The small GPS dry bias at Seychelles (−0.1 mm) may be related to a less reliable sonde PW adjustment at this site to account for a large sensor height difference (537 m). The overall mean GPS minus sonde PW difference among these 11 sites is −1.5 mm (or ~3%). While this difference is within the range of measurement uncertainty,[8] the consistent negative GPS bias among the sites together with the excellent agreement of the sonde and MWR estimates suggests that the GPS PW estimates are, in fact, too low. GPS PW dry biases have been noted in previous

[7] Cycle for heated humidity instrument consisted of 40 s of heating followed by a 20-s cooldown period.

[8] Based on the GRUAN uncertainty analysis for moisture, the uncertainty of the mean PW was ~4.5% for the three DYNAMO sites with GRUAN-processed data.

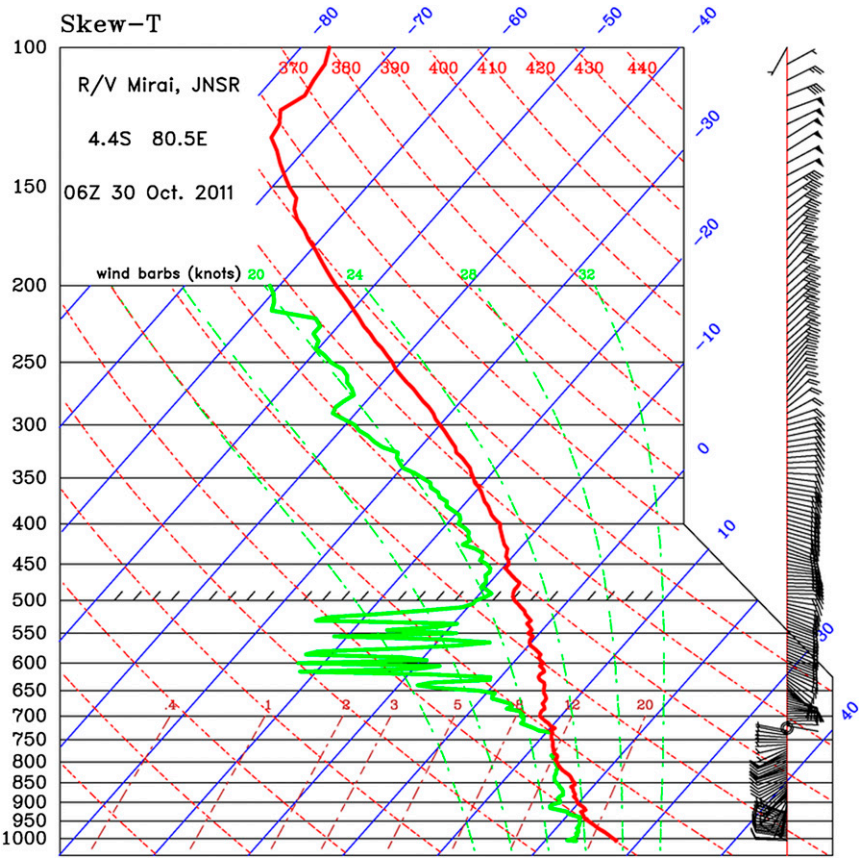

FIG. 13. Skew T plot from R/V *Mirai* for 0600 UTC 30 Oct 2011 showing suspicious T_d data in the layer from 650 to 500 hPa. The ascent rate of the sonde in this layer was ~2.5 m s^{-1}, which resulted in poor ventilation of the sonde humidity sensor and artificial dry spikes in the moisture profile (see text for further explanation).

studies (e.g., Rocken et al. 1993; Tregoning et al. 1998; Wang et al. 2007). While future studies using GPS PW should be aware of its dry bias, understanding the reasons for it are beyond the scope of this study.

To evaluate the impact of the humidity corrections on some basic convective parameters, Table 6 lists the mean values of PW, CAPE, and CIN for the six core DYNAMO sites. Here CAPE and CIN were calculated assuming pseudoadiabatic ascent using mean thermodynamic conditions in the lowest 50 hPa. For comparison with another tropical experiment in which humidity corrections were carried out, values for TOGA COARE are also listed. As one can see, total moisture is higher in the COARE domain, consistent with the higher SSTs there, which results in higher CAPE and lower CIN. The impact of the humidity corrections is an order of magnitude smaller in DYNAMO than in COARE. In DYNAMO the corrections result in a PW increase of 0.3 mm (or 0.6%), and CAPE and CIN increases of 75 J kg^{-1} and 6 J kg^{-1}, respectively. In contrast, the PW increase from corrections of COARE soundings is 3.0 mm (or 5.6%) with CAPE and CIN increases of 450 J kg^{-1} and 17 J kg^{-1}, respectively. Similar large impacts from corrections were observed at many sites in the Terrain-influenced Monsoon Rainfall Experiment (TiMREX; Ciesielski et al. 2010).

b. *Evaluation of satellite and model humidity*

The high quality and accuracy of the sonde moisture data, as demonstrated above, make them a useful tool for validating moisture analyses from other sources. Since satellite retrievals of PW have become increasingly utilized in recent years and are important for research and forecast applications of the water cycle, we examine the microwave-based MIRS PW product, whose high temporal and spatial resolution make it convenient for comparison to sonde data. Figure 15 shows a comparison of contemporaneous sonde and MIRS PW at several sites in the DYNAMO domain. For these comparisons the ~0.1°-resolution, hourly MIRS data were averaged in

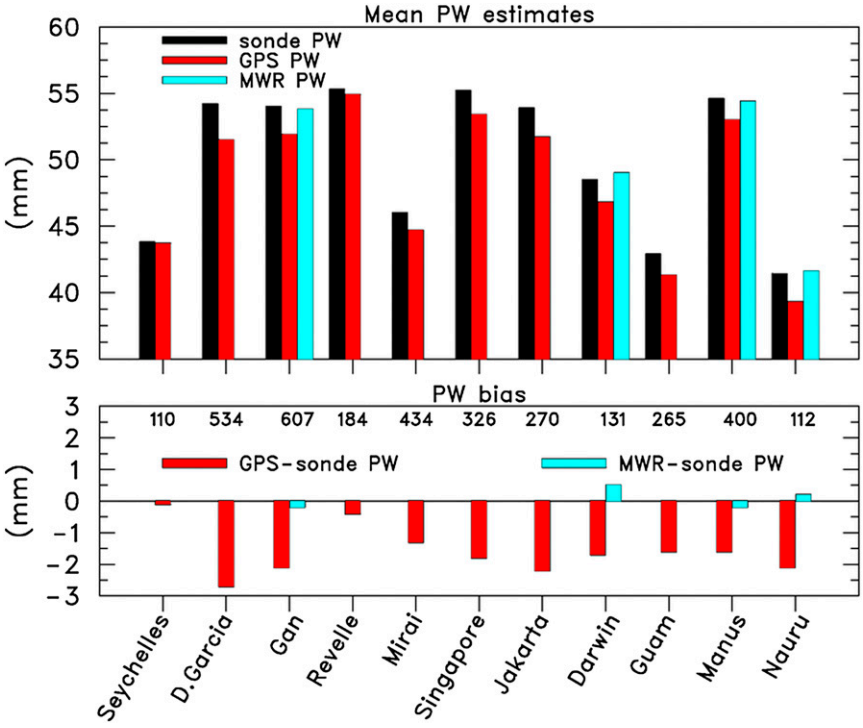

FIG. 14. PW estimates for several sites in the DYNAMO domain, listed from west to east, from sonde (black bar), GPS (red bar) and MWR (cyan bar). (top) Mean for times when all estimates at a given site were available during the EOP. (bottom) shows PW bias defined as independent PW estimate minus sonde estimate. Numbers along top of panel indicate the number of comparisons that went into means.

a circle with a 0.5° radius centered on the sounding site location. At the majority of the sites, the mean MIRS PW bias is <1.0 mm. Sites with higher biases are generally coastal sites on larger landmasses, where PW gradients are large due to complex topographic features (see mean PW map in Fig. 16). At 12 of the 13 sites examined, MIRS exhibits a dry bias relative to the sonde data with an overall mean bias of −1.8 mm. The magnitude of this bias is similar to that reported in Boukabara et al. (2010), in which a global multisite operational sonde and MIRS comparison was conducted; however, their analysis showed the MIRS being moister than the sonde. Since a large fraction of rawinsondes used globally are characterized by a dry bias (Wang and Zhang 2008), the MIRS moist bias found in their study may be related, in part, to their use of uncorrected sonde data. Sonde and MIRS PW standard deviations are quite similar at most sites and temporal correlations range from 0.55 to 0.91. It also worth noting that even at sites with small mean biases, comparisons over the diurnal cycle show considerably more scatter (not shown), such that MIRS does not appear to be a useful tool for studying details of the diurnal cycle at open-ocean sites like Gan, which exhibits a small diurnal variations in PW (see Fig. 5).

As seen in Fig. 16, the meridional width of the equatorial moist tongue varies considerably over the DYNAMO domain with a general west-to-east increase. The narrowness of the moist tongue over the IO may make equatorial sites in this region more susceptible to the dry air intrusions than in the western Pacific (Yoneyama and Parsons 1999). The time series of PW at the six core DYNAMO sites (Fig. 17) show a modulation on the time

TABLE 6. Convective parameter [CAPE (J kg^{-1}), CIN (J kg^{-1}), and PW (mm)] statistics for six core DYNAMO sites for 1 Oct–31 Dec 2011 and four TOGA COARE intensive flux array (IFA) sites for its 4-month IOP, showing range of mean site values, multisite mean, and impact of humidity correction on the parameter.

	DYNAMO core sites	TOGA COARE IFA sites
PW range	46.4 to 55.1	52.0 to 55.1
PW mean	51.7	53.3
PW correction	+0.3	+3.0
CAPE range	846 to 1499	1235 to 1529
CAPE mean	1207	1529
CAPE correction	+75	+450
CIN range	−91 to −42	−43 to −28
CIN mean	−61	−34
CIN correction	+6	+17

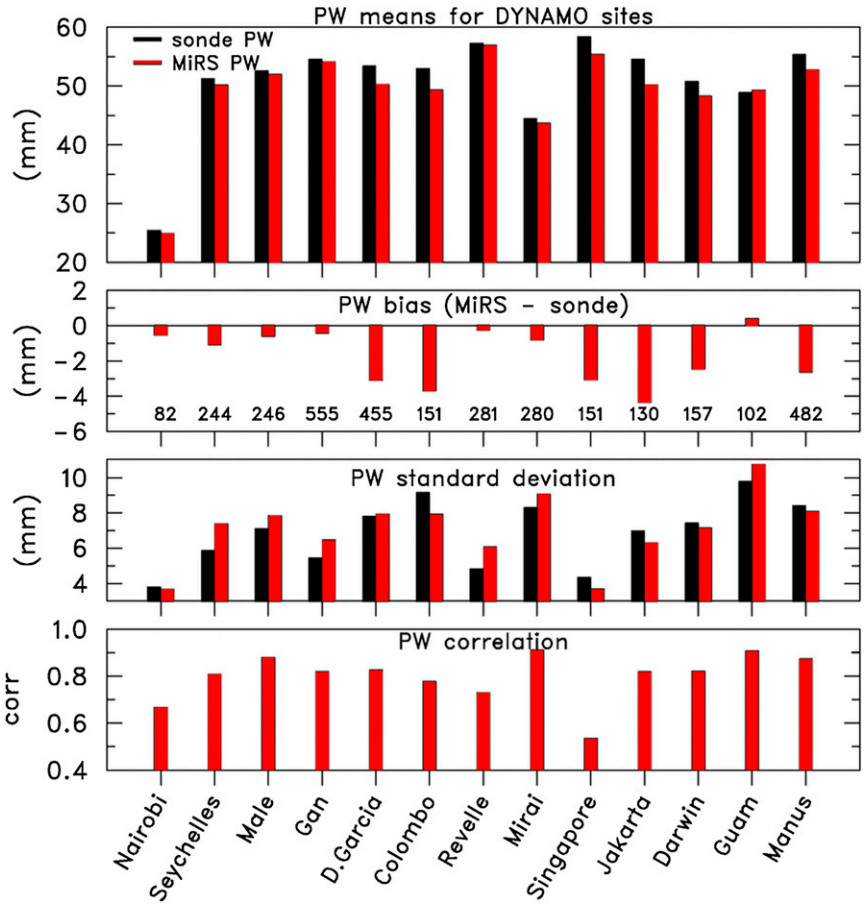

FIG. 15. Comparison of sonde PW statistics to MIRS PW (sonde—black bars, MIRS—red bars) for 13 DYNAMO sites listed from west to east for period 1 Oct–31 Dec 2011: (top to bottom) PW means; PW difference, where negative values imply a MIRS dry bias; PW standard deviations; and temporal correlation coefficient of sonde PW estimates to the MIRS product. Numbers in second panel indicate the number of comparisons that went into statistics at each site.

scale of the MJO. Dry periods are more pronounced at off-equatorial sites like Malé and Colombo. Also, the variation of PW on the MJO time scale is more pronounced for the NSA sites. This is consistent with the findings of Johnson and Ciesielski (2013), who showed a strong modulation of precipitation over the northern array, whereas the southern array experienced more persistent, yet briefer, periods of rainfall mostly related to ITCZ convection.

Because of the wide use of operational and reanalysis products (in process studies, initializing numerical simulations, construction of large-scale forcing datasets for cloud-resolving models, etc.), establishing their validity is important. Preliminary comparisons of ECMWF and GFS operational analyses (OA) to sonde data show excellent agreement in the basic fields (Johnson and Ciesielski 2013). Here we consider a more detailed look at OA humidity fields. Figures 18 and 19 compare mean RH profiles based on sonde and OA data for two near-equatorial DYNAMO sites: Gan and Singapore. A comparison was also performed at Manus (in the western Pacific warm pool), but is not shown due to its similarity to the Gan analyses. Mean profiles were constructed from times during the period 1 October–31 December 2011, when both sonde and OA products were available. At these sites and Manus, the mean OA PWs (shown in parentheses in Figs. 18 and 19) are within 1 mm of the sonde-corrected PWs. Both sonde and OA products captured a significant increase in moisture between Gan, which lies near the western edge of the warm pool, and Singapore, which lies about 30° farther east within the Maritime Continent. This moisture gradient from the IO to the Maritime Continent is consistent with the fact that DYNAMO occurred during a La Niña when positive SST anomalies were present over the Maritime Continent and the western Pacific (Johnson and Ciesielski 2013).

The ECWMF RH profiles show better overall agreement with corrected sounding profiles than those from

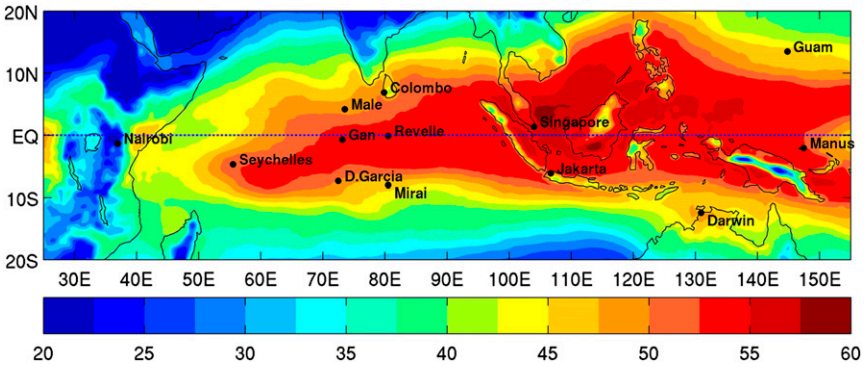

FIG. 16. Mean PW (mm) based on MIRS analyses for the period 1 Oct–31 Dec 2011. Locations of DYNAMO sounding sites examined in Fig. 15 are shown.

the GFS. The GFS profiles have a notable dry bias relative to the sonde data in the boundary layer and a moist bias near 750 hPa. These biases in the GFS are suggestive of an overactive shallow cumulus parameterization scheme that removes too much boundary layer moisture and deposits it above 800 hPa. On the other hand, both OA products are too moist above 300 hPa, which leads to an overestimate in the frequency of saturated layers. The upper-level moist bias is more pronounced in the GFS data with more than double the frequency of saturated layers at Gan and Manus than observed in the corrected sonde data. At Singapore the frequency of

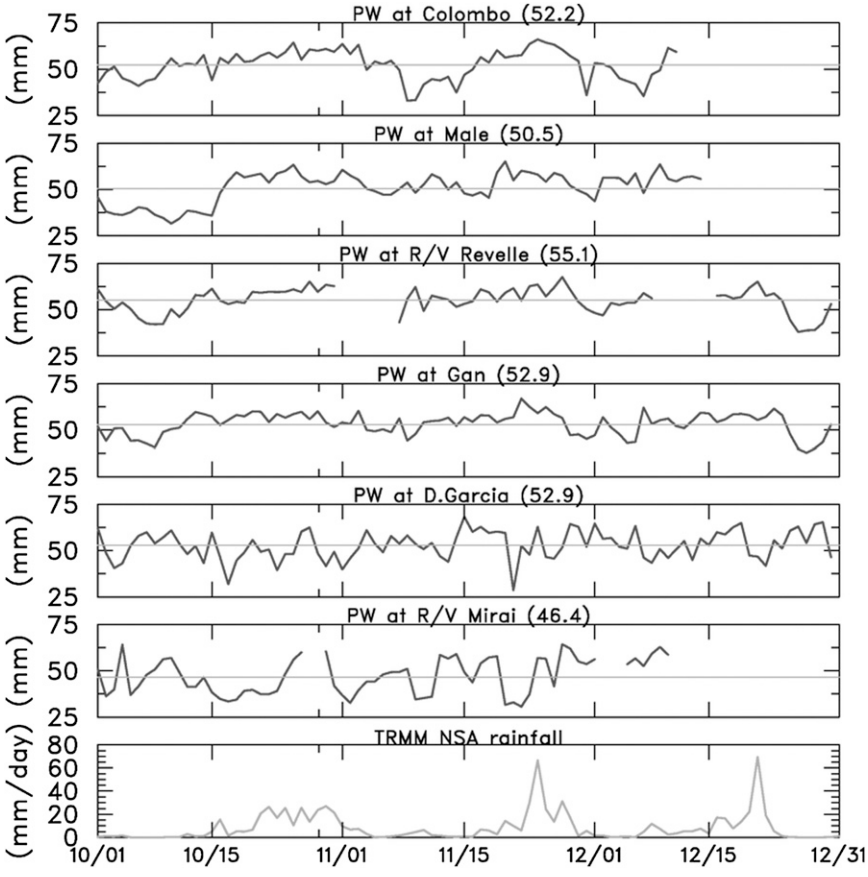

FIG. 17. (top) Daily averaged PW time series for six core sites, and (bottom) TRMM 3B42 rainfall averaged over the NSA. Mean PW is shown by thin gray line and is listed in parentheses.

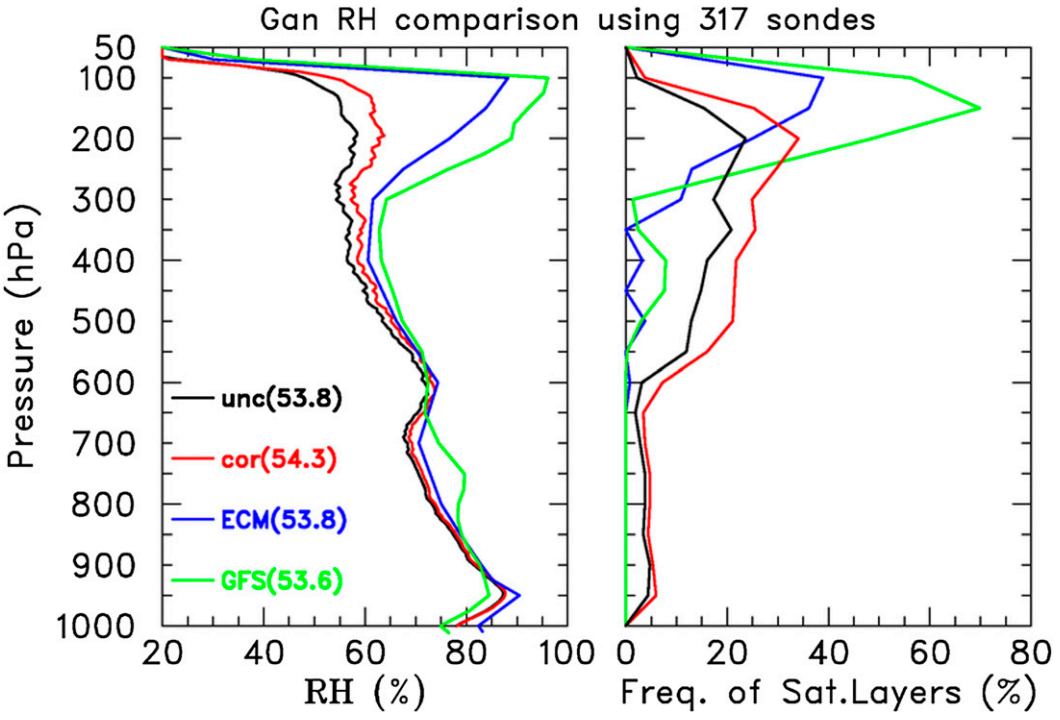

FIG. 18. (left) Comparison of sonde and model mean RH profiles at Gan for the period 1 Oct–31 Dec 2011 computed with soundings from all hours of a 24-h day for (black) uncorrected soundings, (red) D3.64 corrected soundings, (blue) ECMWF, and (green) GFS data, where model data were interpolated to the Gan location. Numbers in parentheses represent period mean PW. (right) Frequency of saturated layers (RH $\geq$ 100%) in 50-hPa layers. Analysis based on RH computed with respect to ice for $T < 0°$.

upper-level saturated layers is comparable between the corrected sondes and ECMWF analysis. Model temperature biases at upper levels at Gan (i.e., a cool bias of 1°C at 100 hPa and a warm bias of 0.5°C at 200 hPa relative to sonde data, not shown) likely reflect radiative feedbacks related to the enhanced model moisture and cloudiness between 100 and 200 hPa (Ackerman et al. 1988).

Comparison of sonde and OA PW at several DYNAMO sites (Fig. 20) shows agreement within the uncertainty of the sonde instruments. To facilitate this comparison, the OA were linearly interpolated to the sounding locations. Except at Nairobi, where the models exhibit a moist bias of 3%–7%, the OA PWs generally exhibit a small dry bias relative to the corrected sonde data. Part of the reason for the model dry bias at some sites could be attributed to assimilation of uncorrected sonde data in the models. For example, at Diego Garcia, which shows the largest model dry bias, the nighttime PW ECMWF bias is −1.8 mm, whereas the daytime bias (based on uncorrected soundings) is −2.9 mm. On the other hand, at Manus corrected soundings were available for assimilation in real time, yet the OA products still show a dry bias of 3%–4% at this site. Finally, small standard deviations of sonde and model PW differences and high correlations (>0.9 except at Singapore) suggest that the OA products have done an excellent job in capturing the temporal variability of moisture during DYNAMO.

6. Summary and concluding remarks

In terms of performance, considering both quantity and quality of upper-air sonde observations, operations in DYNAMO should be considered an extraordinary success. The upper-air sounding network for DYNAMO, which covered the tropics from eastern Africa to the western Pacific, included 72 sounding sites and dropsonde data from 13 aircraft missions. In total 25 938 soundings were collected from this network during the experiment's 6-month extended observing period. This number includes 13 074 high-vertical-resolution soundings from 33 sites. Six core sounding sites in the central Indian Ocean formed two sounding quadrilaterals, one north and one south of the equator. These arrays were intact for the majority of the 1 October–30 November 2011 period, during which time two prominent MJOs passed through the sounding network. Sonde data from these core sites, as well as the larger network, will provide key observations for testing many of the DYNAMO hypotheses.

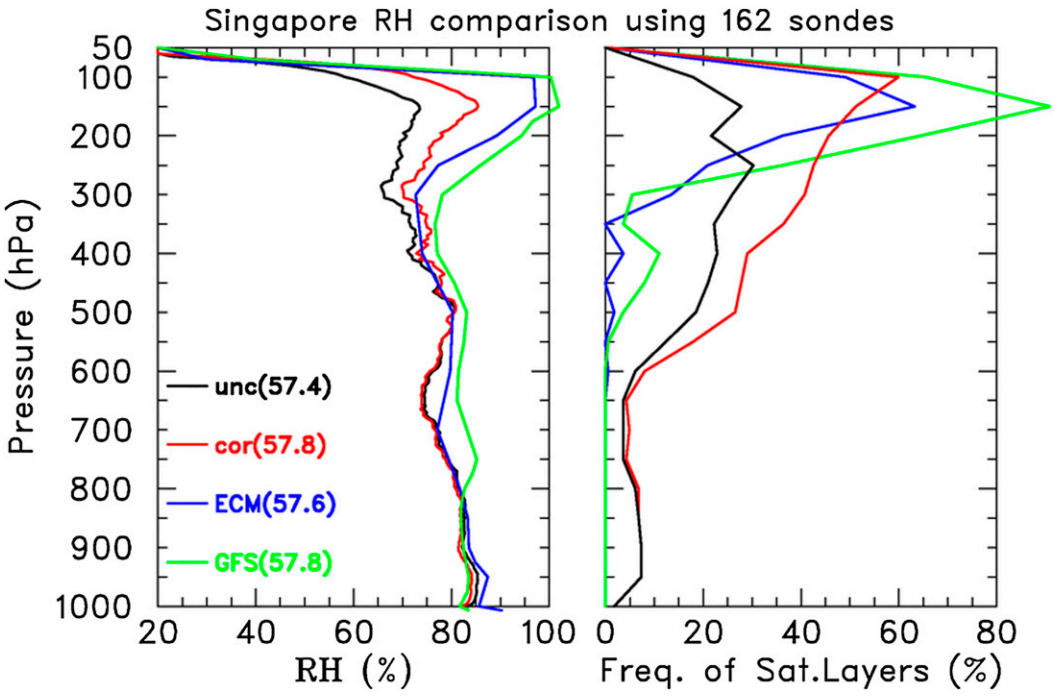

FIG. 19. As in Fig. 18, but at Singapore for period 1 Oct–21 Dec 2011. Here VRS92 sonde humidity was corrected using the NRBC algorithm.

Rigorous post–field phase processing of the sonde data included several levels of quality checks and a variety of corrections that address a number of issues (e.g., daytime time dry bias, errors in baseline surface data, ship deck heating effects, and artificial dry spikes in slow-ascent sondes). Because of the importance of having accurate moisture analyses, a significant portion of the post-processing activities was directed toward improving the quality of the humidity observations. Five of the six core sites used research-quality Vaisala RS92 sondes. Small humidity biases in these sondes were further reduced by the application of additional corrections. While corrections are possible only at sites with hi-res data, sonde data from all sites were processed with QC checks and visual inspection to assign QC flags to each variable. Part of the challenge of correcting the hi-res data is that six different sonde types were involved. Using a variety of techniques, hi-res sonde data from 30 sites were corrected to the standard of reference sondes. Evaluation of corrected sonde data using independent estimates of PW at several key sites showed mean PW biases of 0.5 mm or less, which is well within the uncertainty limits of these sensors. Compared with previous experiments such as TOGA COARE, the humidity corrections applied in DYNAMO produced only small changes in the moisture field (e.g., mean PW for the six core sites increased ~0.3 mm).

In evaluating the sonde moisture data at 11 sites in the extended DYNAMO domain, a small but consistent dry bias (ranging from −0.1 to −2.7 mm) was noted in the GPS PW relative to the sonde and MWR PWs. In this moist environment with mean PWs between 42 and 55 mm, the overall GPS minus sonde PW difference among these 11 sites is −1.5 mm (or ~3%). At present the reasons for this GPS dry bias are unclear. While beyond the scope of this study, understanding the causes for this dry bias is important because of the wide use of GPS PW data in many weather and climate applications.

During the field phase of the experiment, a major effort was undertaken to ensure the real-time transmission of the DYNAMO sonde data onto the GTS for dissemination to the operational NWP centers, which led to a 95% assimilation success rate. A comparison of moisture products using corrected soundings and operational analyses from ECMWF and GFS models shows an overall good agreement with a slight model PW dry bias at most locations. Notable differences occur at upper levels, where model moisture and clouds are more abundant than the sounding data would indicate.

In addition to the corrections described herein, work is in progress to correct for influences of the Sri Lanka island flow blocking and the diurnal cycle on low-level fields in the Colombo soundings.[9] Unless corrected, the large spacing

[9] A north–south mountain range lies ~100 km to the east of the Colombo sonde site with peak elevations over 2500 m.

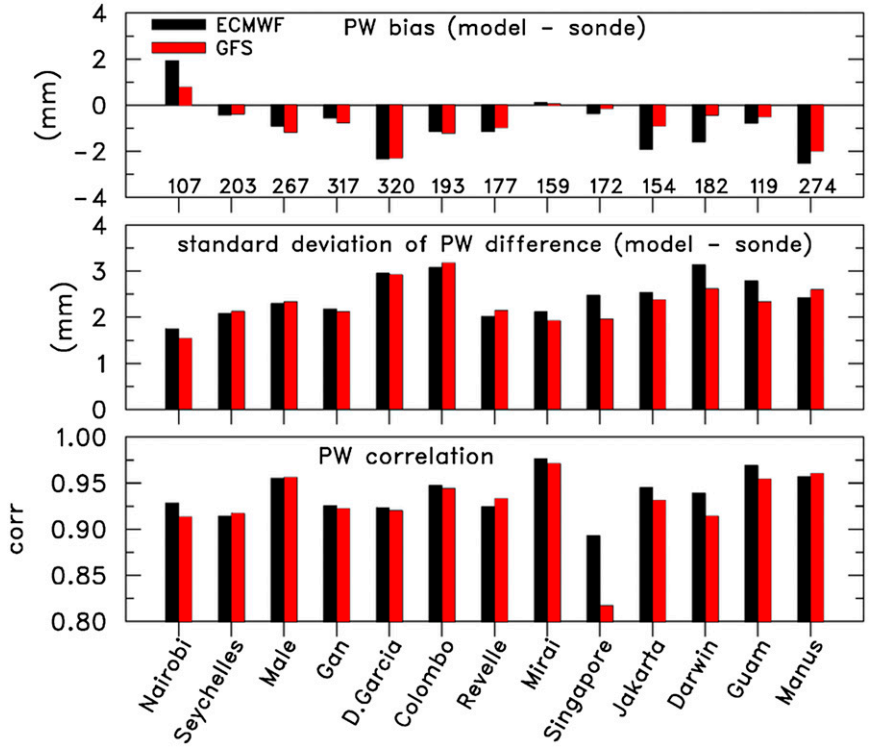

FIG. 20. Comparison of sonde PW statistics to OA PW (ECMWF—black bars, GFS—red bars) for 13 DYNAMO sites listed from west to east for period 1 Oct–31 Dec 2011. (top) Difference in PW means (model minus sonde), where negative values imply a model dry bias, (middle) standard deviation of PW difference, (bottom) temporal correlation coefficient of sonde PW estimates to OA products. Numbers in top panel indicate the number of comparisons that went into statistics at each site.

between sounding sites (see Fig. 1) causes these island-scale effects to be aliased onto larger scales, adversely impacting fields and budget analyses over the NSA. Other islands in the DYNAMO core sounding domain (Malé, Gan, and Diego Garcia) are quite small ($<10\,km^2$) and have only a slight, yet detectable, impact on sonde observations. Efforts are underway primarily using dropsonde data to quantify the impact of these smaller islands.

All sonde data described herein, including documentation describing the processing performed at each site, are available from the EOL DYNAMO data archive online (http://data.eol.ucar.edu/master_list/?project=DYNAMO).

Acknowledgments. The success of the sounding operations for DYNAMO is due to countless students, staff, and scientists from many agencies and universities in Japan, Taiwan, the Maldives, and the United States. In particular, we thank the Maldivian Meteorological Service for their unfailing help during field operations. We also acknowledge support from Pay-Liam Lin of National Central University, and Ben Jong-Dao Jou and Po-Hsuing Lin of National Taiwan University for their assistance with supporting equipment and student staffing at Malé. Enhancement of sounding operations at Seychelles, Nairobi, and Colombo were made possible by local staff collaborations as well as financial assistance from the WMO and JMA. We greatly appreciate the efforts of Jim Moore and his team at NCAR EOL for their guidance and logistical support of sounding operations during the experiment. We also thank Eric DeWeaver and Brad Smull of the National Science Foundation for supporting sounding operations at Malé, Wayne Schubert and Rick Taft for the several insightful discussions; Holger Vömel and Ruud Dirksen for making available the GRUAN-corrected Vaisala data; John Forsythe and Stan Kidder for providing the MIRS PW data; ECMWF for making available its operational analyses; and the WMO for allowing us to use its eighth sonde intercomparison dataset. Finally, special appreciation is extended to Chidong Zhang for his exceptional efforts in orchestrating and implementing DYNAMO. This research has been supported by the National Science Foundation under Grants AGS-1059899 and AGS-1138353. Dr. Long acknowledges support from the Office of Science of the U.S. Department of Energy as part of the ARM and Atmospheric System Research (ASR) programs.

REFERENCES

Ackerman, T. P., K.-N. Liou, F. P. J. Valero, and L. Pfister, 1988: Heating rates in tropical anvils. *J. Atmos. Sci.,* **45,** 1606–1623, doi:10.1175/1520-0469(1988)045<1606:HRITA>2.0.CO;2.

Bock, O., and M. Nuret, 2009: Verification of NWP model analyses and radiosonde humidity data with GPS precipitable water vapor estimates during AMMA. *Wea. Forecasting,* **24,** 1085–1101, doi:10.1175/2009WAF2222239.1.

——, M.-N. Bouin, A. Walpersdorf, J. P. Lafore, S. Janicot, F. Guichard, and A. Agusti-Panareda, 2007: Comparison of ground-based GPS precipitable water vapour to independent observations and NWP model reanalysis over Africa. *Quart. J. Roy. Meteor. Soc.,* **133B,** 2011–2027, doi:10.1002/qj.185.

Boukabara, S.-A., K. Garrett, and W. Chen, 2010: Global coverage of total precipitable water using a microwave variational algorithm. *IEEE Trans. Geosci. Remote Sens.,* **48,** 3608–3621, doi:10.1109/TGRS.2010.2048035.

Cadeddu, M. P., J. C. Liljegren, and D. D. Turner, 2013: The Atmospheric Radiation Measurement (ARM) program network of microwave radiometers: Instrumentation, data, and retrievals. *Atmos. Meas. Tech.,* **6,** 2359–2372, doi:10.5194/amt-6-2359-2013.

Cady-Pereira, K. E., M. W. Shephard, D. D. Turner, E. J. Mlawer, S. A. Clough, and T. J. Wagner, 2008: Improved daytime column-integrated precipitable water vapor from Vaisala radiosonde humidity sensors. *J. Atmos. Oceanic Technol.,* **25,** 873–883, doi:10.1175/2007JTECHA1027.1.

Ciesielski, P. E., and Coauthors, 2010: Quality controlled upper-air sounding dataset for TiMREX/SoWMEX: Development and corrections. *J. Atmos. Oceanic Technol.,* **27,** 1802–1821, doi:10.1175/2010JTECHA1481.1.

——, P. T. Haertel, R. H. Johnson, J. Wang, and S. M. Loehrer, 2012: Developing high-quality field program sounding datasets. *Bull. Amer. Meteor. Soc.,* **93,** 325–336, doi:10.1175/BAMS-D-11-00091.1.

Fujita, M., F. Kimura, K. Yoneyama, and M. Yoshizaki, 2008: Verification of precipitable water vapor estimated from ship-borne GPS measurements. *Geophys. Res. Lett.,* **35,** L13803, doi:10.1029/2008GL033764.

Immler, F. J., and M. Sommer, 2011: Brief description of the RS92 GRUAN data product (RS92-GDP). GRUAN Tech. Doc. GRUAN-TD-4, 17 pp. [Available online at http://www.dwd.de/bvbw/generator/DWDWWW/Content/Projekte/Gruan/Downloads/documents/gruan-td-4,templateId=raw,property=publicationFile.pdf/gruan–4.pdf.]

——, J. Dykema, T. Gardiner, D. N. Whiteman, P. W. Thorne, and H. Vömel, 2010: A guide for upper-air reference measurements: Guidance for developing GRUAN data products. *Atmos. Meas. Tech. Discuss.,* **3,** 1217–1231, doi:10.5194/amt-3-1217-2010.

International and Scientific Management Group of GATE, 1974: GATE final international scientific plans. *Bull. Amer. Meteor. Soc.,* **55,** 711–744, doi:10.1175/1520-0477(1974)055<0711:G>2.0.CO;2.

Johnson, R. H., and P. E. Ciesielski, 2013: Structure and properties of Madden–Julian oscillations deduced from DYNAMO sounding arrays. *J. Atmos. Sci.,* **70,** 3157–3179, doi:10.1175/JAS-D-13-065.1.

Kidder, S. Q., and A. S. Jones, 2007: A blended satellite total precipitable water product for operational forecasting. *J. Atmos. Oceanic Technol.,* **24,** 74–81, doi:10.1175/JTECH1960.1.

Liou, Y., Y. Teng, T. V. Hove, and J. C. Liljegren, 2001: Comparison of precipitable water observations in the near tropics by GPS, microwave radiometer, and radiosondes. *J. Appl. Meteor.,* **40,** 5–15, doi:10.1175/1520-0450(2001)040<0005:COPWOI>2.0.CO;2.

Loehrer, S. M., T. A. Edmands, and J. A. Moore, 1996: TOGA COARE upper-air sounding data archive: Development and quality control procedures. *Bull. Amer. Meteor. Soc.,* **77,** 2651–2671, doi:10.1175/1520-0477(1996)077<2651:TCUASD>2.0.CO;2.

Long, C. N., and D. J. Holdridge, 2012: Investigations of possible low-level temperature and moisture anomalies during the AMIE field campaign on Manus Island. U.S. Department of Energy Tech. Rep. DOE-SC/ARM-TR-119. [Available online at www.arm.gov/publications/tech_reports/doe-sc-arm-tr-119.pdf.]

Miloshevich, L. M., H. Vömel, D. N. Whitman, and T. Leblanc, 2009: Accuracy assessment and correction of Vaisala RS92 radiosonde water vapor measurements. *J. Geophys. Res.,* **114,** D11305, doi:10.1029/2008JD011565.

Nash, J., T. Oakley, H. Vömel, and W. Li, 2011: WMO intercomparisons of high quality radiosonde systems. Instruments and Observing Methods Rep. 107, WMO Tech. Doc. WMO/TD-1580, 238 pp. [Available online at https://www.wmo.int/pages/prog/www/IMOP/publications/IOM-107_Yangjiang/IOM-107_Yangjiang.zip.]

Nuret, M., J.-P. Lafore, F. Guichard, J.-L. Redelsperger, O. Bock, A. Agusti-Panareda, and J.-B. N'Gamini, 2008: Correction of humidity bias for Vaisala RS80-A sondes during the AMMA 2006 observing period. *J. Atmos. Oceanic Technol.,* **25,** 2152–2158, doi:10.1175/2008JTECHA1103.1.

Rocken, C., R. H. Ware, T. Van Hove, F. Solheim, C. Alber, and J. Johnson, 1993: Sensing atmospheric water vapor with the global positioning system. *Geophys. Res. Lett.,* **20,** 2631–2634, doi:10.1029/93GL02935.

——, J. M. Johnson, T. M. Van Hove, and T. Iwabuchi, 2005: Atmospheric water vapor and geoid measurements in the open ocean with GPS. *Geophys. Res. Lett.,* **32,** doi:10.1029/2005GL022573.

Seidel, D. J., and Coauthors, 2009: Reference upper-air observations for climate: Rationale, progress, and plans. *Bull. Amer. Meteor. Soc.,* **90,** 361–369, doi:10.1175/2008BAMS2540.1.

Steigenberger, P., M. Rothacher, R. Dietrich, M. Fritsche, A. Rülke, and S. Vey, 2006: Reprocessing of a global GPS network. *J. Geophys. Res.,* **111,** B05402, doi:10.1029/2005JB003747.

Sugidachi, T., and M. Fujiwara, 2013: Correction of the stepwise change observed at 0°C in Meisei RS2-91, RS-01G, and RS-06G radiosonde relative humidity profiles. *J. Meteor. Soc. Japan,* **91,** 323–336, doi:10.2151/jmsj.2013-306.

Thomas, I. D., M. A. King, P. J. Clarke, and N. T. Penna, 2011: Precipitable water vapor estimates from homogeneously reprocessed GPS data: An intertechnique comparison in Antarctica. *J. Geophys. Res.,* **116,** D04107, doi:10.1029/2010JD013889.

Tregoning, P., R. Boers, D. O'Brien, and M. Hendy, 1998: Accuracy of absolute precipitable water vapor estimates from GPS observations. *J. Geophys. Res.,* **103,** 28 701–28 710, doi:10.1029/98JD02516.

Vaisala, cited 2011: Sounding data continuity. [Available online at http://www.vaisala.com/en/products/soundingsystemsandradiosondes/soundingdatacontinuity/Pages/default.aspx.]

Vömel, H., and Coauthors, 2007: Radiation dry bias of the Vaisala RS92 humidity sensor. *J. Atmos. Oceanic Technol.,* **24,** 953–963, doi:10.1175/JTECH2019.1.

Wang, J., and L. Zhang, 2008: Systematic errors in global radiosonde precipitable water data from comparisons with ground-based GPS measurements. *J. Climate,* **21,** 2218–2238, doi:10.1175/2007JCLI1944.1.

——, H. L. Cole, D. J. Carlson, E. R. Miller, K. Beierle, A. Paukkunen, and T. K. Laine, 2002: Corrections of humidity measurement errors from the Vaisala RS80 radiosonde—Application to TOGA COARE data. *J. Atmos. Oceanic Technol.,* **19,** 981–1002, doi:10.1175/1520-0426(2002)019<0981:COHMEF>2.0.CO;2.

——, L. Zhang, A. Dai, T. Van Hove, and J. Van Baelen, 2007: A near-global, 2-hourly data set of atmospheric precipitable water from ground-based GPS measurements. *J. Geophys. Res.,* **112,** D11107, doi:10.1029/2006JD007529.

——, ——, ——, F. Immler, M. Sommer, and H. Vömel, 2013: Radiation dry bias correction of Vaisala RS92 humidity data and its impact on historical radiosonde data. *J. Atmos. Oceanic Technol.,* **30,** 197–214, doi:10.1175/JTECH-D-12-00113.1.

Ware, R. H., and Coauthors, 2000: SuomiNet: A real-time national GPS network for atmospheric research and education. *Bull. Amer. Meteor. Soc.,* **81,** 677–694, doi:10.1175/1520-0477(2000)081<0677:SARNGN>2.3.CO;2.

Webster, P. J., and R. Lukas, 1992: TOGA COARE: The Coupled Ocean–Atmosphere Response Experiment. *Bull. Amer. Meteor. Soc.,* **73,** 1377–1416, doi:10.1175/1520-0477(1992)073<1377:TCTCOR>2.0.CO;2.

Wentz, F. J., 1997: A well calibrated ocean algorithm for Special Sensor Microwave Imager. *J. Geophys. Res.,* **102,** 8703–8718, doi:10.1029/96JC01751.

Wu, X., M. W. Moncrieff, and K. A. Emmanuel, 2000: Evaluation of large-scale forcing during TOGA COARE for cloud-resolving models and single-column models. *J. Atmos. Sci.,* **57,** 2977–2985, doi:10.1175/1520-0469(2000)057<2977:EOLSFD>2.0.CO;2.

Yamanaka, M. D., and Coauthors, 2008: HARIMAU radar-profiling network over the Indonesian Maritime Continent: A GEOSS early achievement for hydrological cycle and disaster prevention. *J. Disaster Res.,* **3,** 78–88.

Yanai, M., S. Esbensen, and J. H. Chu, 1973: Determination of bulk properties of tropical cloud clusters for large-scale heat and moisture budgets. *J. Atmos. Sci.,* **30,** 611–627, doi:10.1175/1520-0469(1973)030<0611:DOBPOT>2.0.CO;2.

Yoneyama, K., and D. B. Parsons, 1999: A proposed mechanism for the intrusion of dry air into the tropical west Pacific region. *J. Atmos. Sci.,* **56,** 1524–1546, doi:10.1175/1520-0469(1999)056<1524:APMFTI>2.0.CO;2.

——, M. Hanyu, F. Yoshiura, S. Sueyoshi, and M. Katsumata, 2002: Radiosonde observation from the ship in the tropical region. Report of Japan Marine Science and Technology Center, Rep. 45, 31–39. [Available online at http://www.godac.jamstec.go.jp/catalog/data/doc_catalog/media/shiken45_04.pdf.]

——, C. Zhang, and C. N. Long, 2013: Tracking pulses of the Madden–Julian oscillation. *Bull. Amer. Meteor. Soc.,* **94,** 1871–1891, doi:10.1175/BAMS-D-12-00157.1.

Young, K., J. Wang, W. Brown, and D. Lauritsen, 2013: Dynamics of the Madden–Julian Oscillation (DYNAMO) 2011 quality controlled radiosonde dataset from RV Revelle. Version 1.2, NCAR, 14 pp. [Available online at http://data.eol.ucar.edu/datafile/nph-get/347.099/readme.DYNAMO-2011.GAUS-Revelle-3rdRelease.pdf.]